Acoustic Response Validation of a Finite Cylindrical Shell with Multiple Loading Conditions

Chad Taylor Gallagher

Thesis submitted to the faculty of the Virginia Polytechnic Institute and State University
in partial fulfillment of the requirements for the degree of

Master of Science
In
Mechanical Engineering

Steve C. Southward, Chair

Michael J. Roan

Pablo A. Tarazaga

May 4th, 2018
Blacksburg, VA USA

Keywords: Cylindrical Shell, Distributed Loading

Copyright 2018, Chad Gallagher

Acoustic Response Validation of a Finite Cylindrical Shell with Multiple Loading Conditions

Chad Taylor Gallagher

Abstract

Cylindrical shells are used for a variety of engineering applications such as undersea vehicles and aircraft. The models currently used to determine the vibration characteristics of these shells are often approximated by assuming the shell is infinitely long or has shear-diaphragm boundary conditions. These models also ignore complex loading conditions such as plane waves in favor of point forces or free vibration models. This work expands on the capabilities of these models by examining the acoustic response of a finite length cylinder with flat plate endcaps to multiple types of distributed loading conditions. Starting with the Donnell equations of motion for thin cylinders and the classical plate theory equations of motion for the endcaps, spacial domain displacement field solutions for the shell and plates take an assumed form that includes unknown wave propagation coefficients. These solutions are substituted into stress boundary conditions and continuity equations evaluated at the intersections between the shell and plates. An infinite summation is contained within the boundary conditions and continuity equations which is decoupled, truncated, and compiled in matrix form to allow for the propagation coefficients to be found via a convergent sum of vectors. System responses due to a ring loading and multiple cases of plane waves are studied and validated using a finite element analysis of the system. It is shown that the analytical model matches the finite element model well.

Acoustic Response Validation of a Finite Cylindrical Shell with Multiple Loading Conditions

Chad Taylor Gallagher

General Audience Abstract

Cylindrical shells are used for a variety of engineering applications such as undersea vehicles and aircraft. The mathematical models currently used to determine the motion of the shell use approximate methods that can be inaccurate. Often, these models do not apply to forces such as those involved in sonar signals. This work analyses a new model that examines the vibration of a finite length cylinder with flat plate endcaps to multiple types of forces. Standard theories are used to calculate the vibration of the shell and endcaps where the motion of the shell and plates is assumed to follow a specific pattern. Linear algebra techniques are then used to produce the formulas for the motion of the shell. The vibration of the system is validated using a finite element analysis. It is shown that the mathematical model matches the finite element model well.

Acknowledgements

I would like to thank my advisor Dr. Steve Southward for leading this research effort and guiding me though this project. Also, I would like to thank Dr. Andrew Hull of the US Naval Undersea Warfare Center for his guidance concerning the techniques used in this report. Lastly, I would like to thank my committee members Dr. Michael Roan and Dr. Pablo Tarazaga for their support. This work has been sponsored by the Navy Undersea Research Program at the Office of Naval Research.

Contents

List of Figures

List of Tables

Chapter 1
Introduction and Literature Review

1.1 Introduction

1.1.1 Motivation

Many modern engineering applications utilize cylindrical shell structures such as undersea vehicles, aircraft, and pressure vessels. These systems often rely on cylindrical shells' ability to withstand internal or external pressures causing pressure differences across the shell. It is important that the models used to determine the structural response of these shells be complete and accurate as changes in the system's configuration can cause major changes in the response of the shell. The usage of endcaps to enclose these shells creates complex wave reflections in the shell that are not captured using the shell's equations of motion alone. These complexities are compounded based on the type of loading applied to the structure. Current models fail to consider all of these conditions simultaneously.

This project explores the response of these cylindrical shells enclosed with endcaps to various loading conditions. The model developed here demonstrates the intricacies of the connection between the shell and endcaps as well as the difficulties of implementing the forces due to complex loading conditions. This research effort will serve as a starting point for models involving structural reinforcement, acoustic coatings, various endcap shapes, and full elasticity of the shell and endcaps; however, these goals remain beyond the scope of this project.

1.1.2 Objective

The objective of this project is to create model of a finite length cylindrical shell enclosed by flat plate endcaps subjected to four distributed loading conditions. The loading conditions considered are as follows:

1. Ring loading applied to the outer surface of the shell, symmetric about and propagating along the shell's longitudinal axis

2. Incident plane wave applied to the outer surface of the shell, propagating perpendicular to the shell's longitudinal axis

3. Incident plane wave applied to the outer surface of the endcaps, propagating parallel to the shell's longitudinal axis

4. Incident plane wave applied to the outer surface of the shell and endcaps, propagating at some angle between 0° and 90° relative to the longitudinal axis of the shell

All four of these excitations are applied to a shell and endcap system model constructed using Donnell thin shell theory for the shell, the Navier-Cauchy fully elastic equations of motion for a solid reduced to two dimensions for the in-plane motion of the endcaps, and Kirchhoff-Love plate theory for the out of plane motion of the endcaps which are solved using a wave propagation approach. All four loading conditions are harmonic pressure waveforms. Excitation of this type is required by the solution process used in this project. The first loading type, the ring load, is an unrealistic excitation; however, it is useful for characterization and validation of the system. The second and third loading types are special cases of the fourth loading type that allow for easier computation of the boundary conditions of the system. These three loading conditions are representative of realistic excitations like sonar. In addition to building this model, it will be validated using finite element analysis (FEA).

1.2 Literature Review

Cylindrical shell models have been studied for decades. Acoustics and Vibrations textbooks [1,2] offer analysis of the equations of motion for cylindrical shells, often discussing the effects of simple end boundary conditions [3] such as free or clamped shell ends. This is the first step in studying the vibration of a system and is analogous to the vibration study of beams or strings. Free vibration characteristics of finite shells has been explored for shells with free ends [4] and a number of shell and plate combinations [5,6] using a wave propagation coefficient approach. These studies demonstrate the natural frequencies and mode shapes for the configurations they present. Often, these studies provide visual representations of the mode shapes of their given systems and discuss the consequences of changing the parameters of the shells.

The wave propagation method has been extended to forced vibration of cylindrical shells due to a harmonic point force and is sometimes examined alongside the free vibration of the same shells [7] or as standalone studies [8,9]. These models provide useful displacement field solutions representative of forces such as propulsion systems on undersea craft. The excitations are usually applied at the boundaries between shell and plate components for ease of computation of the boundary conditions but can be applied at any point in the system with some slight modifications the boundary conditions used by the wave propagation method. Two dimensional ring loading conditions have been observed in a similar fashion [10,11]. The solution process for determining the forced response due two dimensional ring forces is exactly the same as the solution process for point forces. This type of loading is more useful for cylindrical cylinder systems attached to other structures such as the curved beam model derived in Hull [11].

Distributed excitations in the form of prescribed stresses or displacements at the shell boundary have been studied for finite length shells [12] although the prescribed values were not based on any input forces. Distributed forces have been applied to both thin shell [13] and thick shell [14,15] models in the form of the loading conditions described in section 1.1.2, but only for infinitely long cylinders. The research outlined in 1.1.2 stops here. Displacement solutions due to more complex loading conditions such as spherical waves originating from a nearby source have only been observed using non-analytical methods on infinitely long cylinders [16] and remain quite scarce compared to the volume of literature available for other less complicated types of excitations.

In most of the cases mentioned, the validation performed uses finite element analysis (FEA) results [7,9-13]. Some of the previous works validate their analytical models by comparing their results to similar, previously validated analytical models [14,15]. This method of validation is useful for developing fully elastic thick shell models based on comparable thin shell models; however, the thin shell validation models have themselves been validated using FEA. Occasionally, models will be validated in a laboratory setting using experimental data. This is clearly the ultimate way to validate a model. It is also the most difficult way to validate a model. For example, the creators of models with external fluid loading such as the one described in Doherty [15] may not have access to an adequate environment to perform the required testing. Fortunately, proper use of FEA methods generates extremely accurate results.

1.3 Chapter Summary

The following outline summarizes the remaining chapters. Chapter 2 will cover the existing literature in more detail. The shell models and excitations along with their advantages and limitations will be discussed with emphasis on how these models compare to the objectives stated

in 1.1.2. The chapter will be organized first by excitations in order of increasing complexity then by increasing complexity of the shell model's configuration. Chapter 3 will derive the shell model described in 1.1.2 and discuss its advantages and limitations. In addition to the mathematics involved, a portion of this chapter will focus on difficulties encountered implementing the model into a Matlab script. Chapter 4 will demonstrate the results of the model and compare them to the FEA validation. Finally, Chapter 5 will present the conclusions of this research effort.

Chapter 2
Survey of Existing Models and Excitations

In order to better discuss the existing models and excitations in the literature, this chapter will have a short overview of the wave propagation method used to determine the displacement field solutions for cylindrical shells. This overview will provide a knowledge basis for the remaining sections in this chapter. A more in depth discussion of the method will be provided in Chapter 3 when the model relevant to this project is derived.

2.1 Overview of the Wave Propagation Method

The wave propagation method for generating displacement field solutions for dynamic systems begins with the equations of motion for the components of the system of interest. For thin cylindrical shells, this often means using Donnell-Mushtari shell theory as is done in this project. Some models use Flügge shell theory which increases the frequency range in which the model is still accurate. Thick shells use the Navier-Cauchy equations of motion for solids. Thin plates have their own set of theories such as Kirchhoff-Love theory, and thick plates also use the Navier-Cauchy equations. Figure 2.1.1 defines the coordinates of the system as r, θ, and x for the radial, tangential, and longitudinal directions; their associated displacements u, v, and w, respectively; and the dimensions of the cylinder where L is the cylinder length, a is the cylinder and plate radii, h is the thickness of the shell, and b is the thickness of the plate. All of these theories generate displacement solutions in cylindrical coordinates of the form

$$u = \sum_{n=0}^{\infty} U_n(r) \cos(n\theta)\, e^{-i\omega t} \qquad 2.1.1$$

where $U_n(r)$ is an unknown wave propagation coefficient. These coefficients generally consist of a sum of number of other unknown coefficients; however, they can be solved for directly in the case of infinitely long thin cylindrical shells. The assumed solution is then inserted into the relevant equations of the shell theory of choice, and an orthogonalization process is used to decouple the individual terms in the summation. The now decoupled terms can be assembled into individual matrix equations of the form $\boldsymbol{Ax} = \boldsymbol{b}$ where $\boldsymbol{A}$ is a square matrix containing the dynamics of the system, $\boldsymbol{x}$ is a vector containing the unknown wave propagation coefficients, and $\boldsymbol{b}$ contains any forces applied to the system. The wave propagation coefficients and therefore the displacement field solutions are solved via $\boldsymbol{x} = \boldsymbol{A}^{-1}\boldsymbol{b}$. This method requires the excitations to be harmonic.

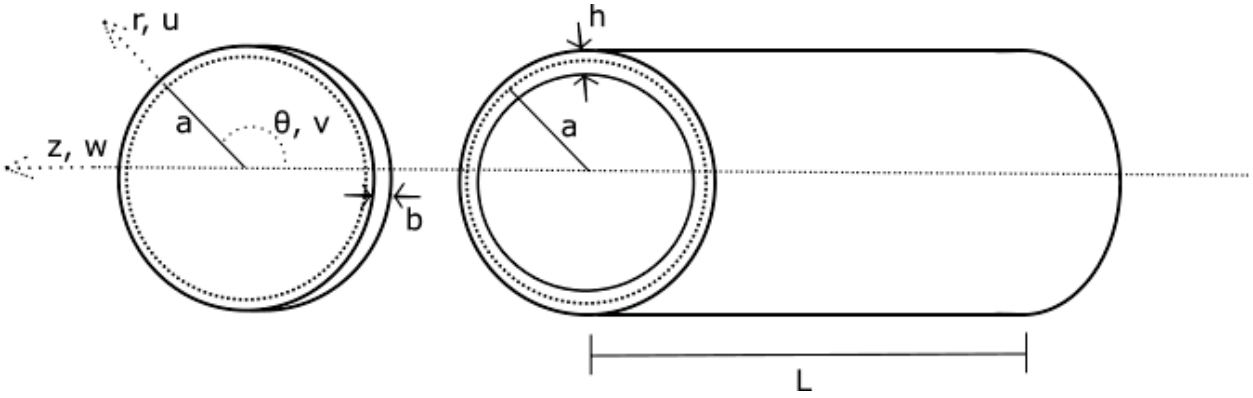

Figure 2.1.1 – Dimensions of the shell.

2.2 Free Vibration Models

The free vibration characteristics of cylindrical shells have been observed for all types of shell models. Determining the free vibration characteristics of any given system is the first step in evaluating the structural response of a system. This analysis reveals the natural frequencies and mode shape. Since solving the matrix equation $Ax = 0$ returns all zero wave propagation coefficients, the natural frequencies are found from the eigenvalues of A.

The advantage of this type of analysis is its ease of validation using modal analysis on physical systems. Comparing the free vibration characteristics of the model to the modal analysis results from the physical provides a straightforward way to validate the accuracy of the theory used to model the system. The result of this comparison is useful for justifying any simplifying assumptions used to create the model. The free vibration case has been performed for all types of cylindrical shell systems including infinitely long shells [17], finite shell and plate systems [5],

and reinforced finite shells [18]. Since the free vibration of cylindrical shells is well studied for the shell and plate theories used in this project, it is not implemented in the model derived in Chapter 3.

The disadvantage of this analysis is its inability to provide insight into the forced response of the system. While the natural frequencies and mode shapes are important design considerations, the steady state forced response of a system is dominated by the excitation frequency. The wave propagation method requires harmonic loading and is intended to find displacement field solutions due to these harmonic loading conditions; therefore, the method is best suited to determine the steady state response of the system.

2.3 Point Excitations

The simplest form of excitation applied to cylindrical shells is in the form of a harmonic point force. Point forces can be used to accurately represent some real world applications, especially internal excitations such as engines in undersea vehicles. These forces have the form

$$F(r,\theta,z,t) = F_0\delta(r-r_0)\delta(\theta-\theta_0)\delta(z-z_0)e^{-i\omega t} \qquad 2.3.1$$

where F_0 is the magnitude of the force, z_0 is the longitudinal location of the force, θ_0 is the tangential location of the force, and r_0 is the radial location of the force. The wave propagation method presented here and in other papers allows the effects of multiple point sources to be applied to a system simultaneously; therefore, effects of an input such as an engine can be characterized as a combination of point forces. This results in accurate displacement field solutions for the cylindrical shell system. This type of loading condition has also been applied to all types of cylindrical shell systems from cylinder only systems [8] to full undersea vehicle models [9].

While point forces are the simplest loading conditions that can be applied to a cylindrical shell, their evaluation is still subject to the same difficulties encountered when evaluating more complex excitations. The wave propagation method's utilization of the matrix form $Ax = b$ where b contains all of the mathematics characterizing any excitations applied to the system does not change the computational requirement of the inverse of A. Also, point forces in existing models are often applied where they are easiest to compute. Applying these forces at connections between pieces of a system or at a free end of a shell allows the same boundary conditions in the free vibration case to be used. Specific orientations of these forces also prevent them from causing moments. Many research papers stop their analysis here despite the minimal effort required to generalize their models to include effects due to any point force. Regardless, the literature contains many examples of point forces applied to cylindrical shell systems, and this loading condition is not considered in this research effort.

An extension of point forces is a two dimensional ring force. This type of force is distributed tangentially about the shell but applied only at a particular longitudinal and radial location. It has the form

$$F(r,\theta,z,t) = F_0\delta(r-r_0)\delta(z-z_0)e^{-i\omega t} \quad 2.3.2$$

When compared to equation 2.3.1, it is clear the two dimensional ring force and point force are mathematically very similar. These forces enter the boundary conditions of the system in the same way as point forces with the difference between them appearing during the orthogonalization step. As with point forces, this type of loading condition is often applied where it causes no moments. This type of loading also exists in some literature [10,11]; therefore, this project does not include two dimensional ring forces in its analysis.

2.4 Ring Loading

As it will be known in this report, ring loading consists of a radial pressure wave applied to the exterior of the shell propagating in the longitudinal direction. It has the form

$$P(r,\theta,z,t) = P_0 e^{ikz} e^{-i\omega t} \quad 2.4.1$$

where P_0 is the magnitude of the pressure wave, k is the excitation wavenumber, and ω is the forcing frequency. This type of excitation is not representative of any realistic loading condition; however, it is useful for characterizing the system response as it only excites the first mode. This type of loading condition is first in the objectives in section 1.1.2 because it has only been applied to various infinitely long cylindrical shell models [13,14,15]. Infinitely long thin shells require three boundary conditions, and infinitely long thick shells require six boundary conditions. These boundary conditions manifest themselves in the form of force balances in the radial, tangential, and longitudinal directions. Any moments due to the ring load can be ignored in the infinitely long shell case. Finite length thin shell models require eight boundary conditions; therefore, the moments due to the ring load must be considered. This type of excitation applied to finite length shells in order to find displacement field solutions has not been studied in other literature and will be discussed in depth in Chapter 3.

2.5 Incident Plane Waves

Incident plane waves consist of waves whose wavefronts are infinite parallel planes. This type of excitation is given in Cartesian coordinates by

$$P_i(x, y, z, t) = P_0 e^{i(\boldsymbol{k}\boldsymbol{r} - \omega t)} \quad 2.5.1$$

where $\boldsymbol{r} = [x, y, z]^T$ is the location vector of the wave and $\boldsymbol{k} = \left[k_x, k_y, k_z\right]^T$ is the vector of excitation wavenumber components in each direction. This type of excitation is a valid approximation for incoming oscillatory signals originating from distant sources such as sonar. Generally, fluids are assumed to not transmit shear forces; therefore, the forces due to plane waves are interpreted as being normal to the surface they are applied. Plane waves can still excite circumferential modes as they are not symmetric about the longitudinal axis of the shell. Similar to the ring load in section 2.4, this type of excitation has been studied for many variations of infinitely long shells [14,15]. Displacement field solutions have not been derived in the finite case. This type of loading condition will also be discussed in depth in Chapter 3.

2.6 Other Loading Conditions

Few other loading conditions have been considered in the literature. In one case [12], a prescribed boundary stress has been studied. This type of loading is not very useful for analyzing the forced response of a system due to an external excitation, but it is useful for characterizing the system. Its purpose is similar to the ring loading condition. Since a ring load is included in this research effort, prescribed stresses have been excluded.

Another type of loading condition found in literature is the spherical wave. As mentioned in section 2.5, incident plane waves are an approximation to spherical waves at long distances from their source. This approximation breaks down as the location where a spherical wave is evaluated approaches the location of its source. One case has determined the effects of spherical waves applied to infinitely long cylinders using a graphical method, but there appears to be no analysis of this interaction using analytical methods. This excitation is beyond the scope of this project.

Chapter 3
Derivation of Model and Excitations

This chapter will cover the theories used for the system model as well as the application of the excitations to the model. The model and ring loading conditions will be covered in the first two sections. Over the next for sections, the plane wave will be derived in cylindrical coordinates, two simplifying special cases of the plane wave will be applied to the model, and the general case of the plane wave will be applied to the model.

3.1 Derivation of Model

The model used in this research effort consists of a cylindrical shell enclosed on each side by flat plates. In this research effort, Donnell thin shell theory is used for the shell, and the plate is governed by two dimensional plane stress equations of motion for the in plane displacement and Kirchhoff-Love plate theory for the out-of-plane displacement. The combination of these theories has previously been used by Hull [11]. This combination has been used here as they are well studied, relatively simple theories which will provide an accurate representation of the system at the frequency range for which the system response will be validated. The following sections will discuss the displacement field solutions for the shell, the displacement field solutions the plate, and the boundary conditions and continuity equations of the system, respectively.

3.1.1 Shell Theory and Displacement Field Solution

Donnell shell theory [19] describes the motion of thin shells using the displacement of the middle surface of the shell. The equations of motion are given in the longitudinal direction as

$$\rho h\frac{\partial^2 u(a,\theta,z,t)}{\partial t^2}-\rho h c_p^2\frac{\partial^2 u(a,\theta,z,t)}{\partial z^2}-\frac{(1-\nu)\rho h c_p^2}{2a^2}\frac{\partial^2 u(a,\theta,z,t)}{\partial \theta^2}$$
$$-\frac{(1+\nu)\rho h c_p^2}{2a}\frac{\partial^2 v(a,\theta,z,t)}{\partial z\partial\theta}-\frac{\nu\rho h\, c_p^2}{a}\frac{\partial w(a,\theta,z,t)}{\partial z}=0 \qquad 3.1.1$$

in the tangential direction as

$$-\frac{(1+\nu)\rho h c_p^2}{2a}\frac{\partial^2 u(a,\theta,z,t)}{\partial z\partial\theta}-\frac{(1-\nu)\rho h c_p^2}{2}\frac{\partial^2 v(a,\theta,z,t)}{\partial z^2}-\frac{\rho h c_p^2}{a^2}\frac{\partial^2 v(a,\theta,z,t)}{\partial \theta^2}$$
$$+\rho h\frac{\partial^2 v(a,\theta,z,t)}{\partial t^2}-\frac{\rho h c_p^2}{a^2}\frac{\partial w(a,\theta,z,t)}{\partial\theta}=0 \qquad 3.1.2$$

and in the radial direction as

$$\frac{\nu\rho h\, c_p^2}{a}\frac{\partial u(a,\theta,z,t)}{\partial z}+\frac{\rho h c_p^2}{a^2}\frac{\partial v(a,\theta,z,t)}{\partial\theta}+\frac{\rho h c_p^2}{a^2}w(a,\theta,z,t)+\frac{\rho h^3 c_p^2}{12}\frac{\partial^4 w(a,\theta,z,t)}{\partial z^4}$$
$$+\frac{\rho h^3 c_p^2}{6a}\frac{\partial^4 w(a,\theta,z,t)}{\partial z^2\partial\theta^2}+\frac{\rho h^3 c_p^2}{12a^4}\frac{\partial^4 w(a,\theta,z,t)}{\partial\theta^4}+\rho h\frac{\partial^2 w(a,\theta,z,t)}{\partial t^2}=0 \qquad 3.1.3$$

where $u(a,\theta,z,t)$ is the longitudinal displacement of the shell, $v(a,\theta,z,t)$ is the tangential displacement of the shell, $w(a,\theta,z,t)$ is the radial displacement of the shell, h is the shell thickness, a is the average shell radius, ρ is the material density, and c_p is the wave speed of the shell material given by

$$c_p=\sqrt{\frac{E}{\rho(1-\nu^2)}} \qquad 3.1.4$$

where E is the modulus of elasticity and ν is Poisson's ratio for the material. The displacement field solutions for the general case of shell boundary conditions have been derived for these equations by Vinson [20] as an infinite summation of circumferential modes. The longitudinal displacement has the form

$$u=\sum_{n=0}^{\infty}\left[\sum_{j=1}^{8}C_j^{(n)}G_j^{(n)}\exp\left(\lambda_j^{(n)}z\right)\right]\sin(n\theta)\exp(-i\omega t) \qquad 3.1.5$$

the torsional displacement has the form

$$v=\sum_{n=0}^{\infty}\left[\sum_{j=1}^{8}C_j^{(n)}H_j^{(n)}\exp\left(\lambda_j^{(n)}z\right)\right]\sin(n\theta)\exp(-i\omega t) \qquad 3.1.6$$

and the radial displacement has the form

$$u = \sum_{n=0}^{\infty} \left[\sum_{j=1}^{8} C_j^{(n)} \exp\left(\lambda_j^{(n)} z\right) \right] \sin(n\theta) \exp(-i\omega t) \tag{3.1.7}$$

where $C_1^{(n)}$ - $C_8^{(n)}$ are unknown wave propagation coefficients for the n^{th} mode of the shell, $\lambda_j^{(n)}$ are the eigenvalues of the n^{th} mode of the shell, ω is frequency, and the constants $G_j^{(n)}$ and $H_j^{(n)}$ are given by

$$G_j^{(n)} = \frac{\lambda_j a c_p^2 \left(\lambda_j^2 a^2 c_p^2 \nu^2 - \lambda_j^2 a^2 c_p^2 \nu - 2\nu a^2 \omega^2 + c_p^2 n^2 \nu - c_p^2 n^2\right)}{\left(\lambda_j^2 a^2 c_p^2 + a^2 \omega^2 - c_p^2 n^2\right)\left(2a^2 \omega^2 - c_p^2 n^2 + c_p^2 n^2 \nu + \lambda_j^2 a^2 c_p^2 - \lambda_j^2 a^2 c_p^2 \nu\right)} \tag{3.1.8}$$

and

$$H_j^{(n)} = \frac{c_p^2 n \left(-\lambda_j^2 a^2 c_p^2 \nu^2 - \lambda_j^2 a^2 c_p^2 \nu + 2\lambda_j^2 a^2 c_p^2 + 2a^2 \omega^2 + c_p^2 n^2 \nu - c_p^2 n^2\right)}{\left(\lambda_j^2 a^2 c_p^2 + a^2 \omega^2 - c_p^2 n^2\right)\left(2a^2 \omega^2 - c_p^2 n^2 + c_p^2 n^2 \nu + \lambda_j^2 a^2 c_p^2 - \lambda_j^2 a^2 c_p^2 \nu\right)} \tag{3.1.9}$$

Note that the n superscript in equations 3.1.8 and 3.1.9 has been removed for visual clarity.

The displacement solution in this form require the eigenvalues of the shell to be found. Since the eigenvalues of the shell are independent of the boundary conditions and externally applied excitations, the eigenvalues are found by inserting equations 3.1.5, 3.1.6, and 3.1.7 into equations 3.1.1, 3.1.2, and 3.1.3. The resulting equations contain the infinite sum of circumferential modes in every term. To decouple the summation terms, the equations can be orthogonalized about θ. The orthogonalization process takes advantage of the orthogonality of trigonometric functions by multiplying the equations by another indexed trigonometric term and integrating the equations over the range of θ. In equation form, this property is written as

$$\int_0^{2\pi} \cos(n\theta) \cos(n_2\theta)\, d\theta = \begin{cases} 1, & n = n_2 \\ 0, & n \neq n_2 \end{cases} \tag{3.1.10}$$

The resulting decoupled equations can be rearranged in the matrix form

$$\boldsymbol{A}\boldsymbol{x} = \boldsymbol{0} \tag{3.1.11}$$

where $\boldsymbol{x}$ contains the unknown wave propagation coefficients and $\boldsymbol{A}$ contains the dynamics of the shell. Setting the determinant of $\boldsymbol{A}$ equal to zero results in the characteristic equation of the system in terms of the circumferential mode number n. The characteristic equation has the form

$$\lambda^8 + a_3\lambda^6 + a_2\lambda^4 + a_1\lambda^2 + a_0 = 0 \tag{3.1.12}$$

where

$$a_3 = \frac{-4a^6 c_p^6 h^2 n^2 (1-\nu) + a^8 c_p^4 h^2 \omega^2 (3-\nu)}{a^8 c_p^6 h^2 (1-\nu)} \tag{3.1.13}$$

$$a_2 = \frac{a^4 c_p^2 \begin{pmatrix} 2a^4h^2\omega^4 - 12a^4c_p^2\omega^2(1-\nu) - 12a^2c_p^4\nu^2(1-\nu) + 12a^2c_p^4(1-\nu) \\ -3a^2c_p^2h^2n^2\omega^2(3-\nu) + 6c_p^4h^2n^4(1-\nu) \end{pmatrix}}{a^8c_p^6h^2(1-\nu)} \quad 3.1.14$$

$$a_1 = \frac{a^2 c_p^2 \begin{pmatrix} 36a^4c_p^2\omega^2 - 4a^4h^2n^2\omega^4 - 12a^6\omega^4(3-\nu) + 24a^4c_p^2n^2\omega^2(1-\nu) \\ -12a^4c_p^2\omega^2\nu(1+2\nu) + 3a^2c_p^2h^2n^4\omega^2(3-\nu) - 4c_p^4h^2n^6(1-\nu) \end{pmatrix}}{a^8c_p^6h^2(1-\nu)} \quad 3.1.15$$

$$a_0 = \frac{\left(2a^2\omega^2 - c_p^2n^2(1-\nu)\right)\begin{pmatrix} -12a^6\omega^4 + 12a^4c_p^2n^2\omega^2 + 12a^4c_p^2\omega^2 \\ +a^2c_p^2h^2n^4\omega^2 - c_p^4h^2n^6 \end{pmatrix}}{a^8c_p^6h^2(1-\nu)} \quad 3.1.16$$

Solving for the 8 roots of equation 3.1.13 reveals the eigenvalues of the shell. The only remaining unknown values in the displacement field solutions of equations 3.1.5 – 3.1.7 are the eight unknown propagation coefficients per circumferential mode.

The wave propagation coefficients will be solved for using equilibrium balances and continuity equations based on the system's configuration and loading conditions. In the wave propagation method, equilibrium balances are constructed using generalized forces and generalized moments. The shell being modeled is assumed to have a thickness much smaller than its radius, and Donnell models the motion of the shell as the displacement of its middle surface. In order to equate internal stresses in the shell, the three dimensional stress states of the physical system must be converted into quasi-two dimensional stress states by integrating the stresses over the thickness of the shell. Figure 3.1.1 shows an infinitesimal element of the shell. The shear generalized force is found by integrating the shear stress of the shell over the thickness of the shell as given by

$$V_z = \int_{-\frac{h}{2}}^{\frac{h}{2}} \sigma_{r\theta}\left(1 + \frac{r}{a}\right) dr \quad 3.1.17$$

The stresses in the system are related to the strains of the system via Hooke's Law which allows the generalized forces to be calculated as functions of displacements. These generalized forces are based on the concept of virtual work. The construction of the generalized forces for Donnell shell theory has been performed by Leissa [3]. Axial, tangential, and radial generalized forces as well as the longitudinal generalized moment are used as boundary conditions in this model and are calculated respectively using the following equations:

$$N_z(a,\theta,z,t) = \frac{Eh}{(1-\nu^2)}\left(\frac{\partial u(a,\theta,z,t)}{\partial z} + \frac{\nu}{a}\frac{\partial v(a,\theta,z,t)}{\partial \theta} + \frac{\nu}{a}w(a,\theta,z,t)\right) \quad 3.1.18$$

$$V_\theta(a,\theta,z,t) = \frac{Eh}{2(1+\nu)}\left(\frac{1}{a}\frac{\partial u(a,\theta,z,t)}{\partial \theta} + \frac{\partial v(a,\theta,z,t)}{\partial z}\right) - \frac{(1-\nu)D}{a^2}\frac{\partial^2 w(a,\theta,z,t)}{\partial z \partial \theta} \quad 3.1.19$$

$$V_z(a,\theta,z,t) = -D_s\left(\frac{\partial^3 w(a,\theta,z,t)}{\partial z^3} + \frac{(2-\nu)}{a^2}\frac{\partial^3 w(a,\theta,z,t)}{\partial z \partial \theta^2}\right) \quad 3.1.20$$

$$M_z(a,\theta,z,t) = -D_s\left(\frac{\partial^2 w(a,\theta,z,t)}{\partial z^2} + \frac{\nu}{a^2}\frac{\partial^2 w(a,\theta,z,t)}{\partial \theta^2}\right) \quad 3.1.21$$

where the flexural rigidity of the shell D_s is defined as

$$D_s = \frac{Eh^3}{12(1-\nu^2)} \quad 3.1.22$$

Note that there is no transverse normal force term as ideal membranes have zero out-of-plane normal stress. The boundary conditions using these generalized forces will be constructed in section 3.1.3.

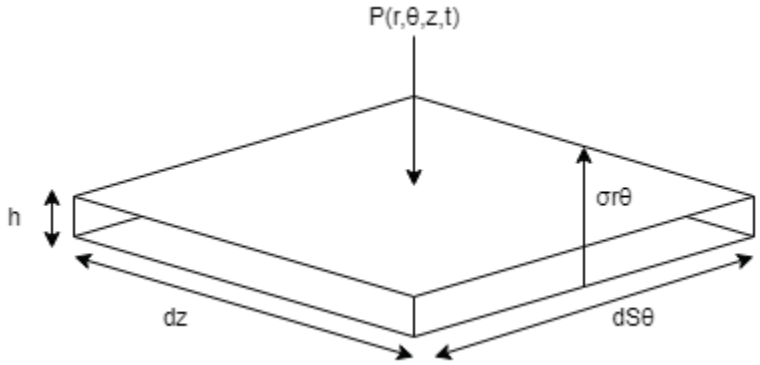

Figure 3.1.1 – Infinitesimally small element of the shell

3.1.2 Plate Theory and Displacement Field Solution

The flat circular plates used as endcaps in the system are modeled using the Navier-Cauchy fully elastic equations of motion reduced to two dimensional plane stress for the in-plane displacement of the plate and Kirchhoff-Love plate theory for the out-of-plane displacement of the plate. The plane stress simplification of the Navier-Cauchy equations of motion is given in Cauchy [21]. Motion of the plate in the radial direction is given by

$$\frac{E}{1-\nu^2}\left(\frac{\partial^2 w(r,\theta,t)}{\partial r^2} + \frac{1}{r}\frac{\partial w(r,\theta,t)}{\partial r} - \frac{1}{r^2}w(r,\theta,t)\right) + \frac{E}{2(1+\nu)}\frac{1}{r^2}\frac{\partial^2 w(r,\theta,t)}{\partial \theta^2}$$
$$-\frac{E(3-\nu)}{2(1-\nu^2)}\frac{1}{r^2}\frac{\partial v(r,\theta,t)}{\partial \theta} + \frac{E}{2(1-\nu)}\frac{1}{r}\frac{\partial^2 v(r,\theta,t)}{\partial r \partial \theta} = \rho\frac{\partial^2 w(r,\theta,t)}{\partial t^2} \quad 3.1.23$$

and motion in the tangential direction is given by

$$\frac{E}{2(1+\nu)}\left(\frac{\partial^2 v(r,\theta,t)}{\partial r^2}+\frac{1}{r}\frac{\partial v(r,\theta,t)}{\partial r}-\frac{1}{r^2}v(r,\theta,t)\right)+\frac{E}{1-\nu^2}\frac{1}{r^2}\frac{\partial^2 v(r,\theta,t)}{\partial \theta^2}$$
$$-\frac{E(3-\nu)}{2(1-\nu^2)}\frac{1}{r^2}\frac{\partial v(r,\theta,t)}{\partial \theta}+\frac{E}{2(1-\nu)}\frac{1}{r}\frac{\partial^2 v(r,\theta,t)}{\partial r\partial \theta}=\rho\frac{\partial^2 v(r,\theta,t)}{\partial t^2} \quad 3.1.24$$

where $w(r,\theta,t)$ is the radial displacement of the plate and $v(r,\theta,t)$ is the tangential displacement of the plate. The solutions for the in-plane motion of the plate has been derived by Graf [2] and is given by

$$v(r,\theta,t)=\sum_{n=0}^{\infty}V_n(r)\sin(n\theta)\exp(-i\omega t) \quad 3.1.25$$

in the tangential direction and

$$w(r,\theta,t)=\sum_{n=0}^{\infty}W_n(r)\cos(n\theta)\exp(-i\omega t) \quad 3.1.26$$

in the radial direction where

$$V_n(r)=-C_9^{(n)}\frac{n}{r}J_n(k_p r)-C_{10}^{(n)}\frac{n}{r}Y_n(k_p r)+C_{11}^{(n)}\left(k_s J_{n+1}(k_s r)-\frac{n}{r}J_n(k_s r)\right)$$
$$+C_{12}^{(n)}\left(k_s Y_{n+1}(k_s r)-\frac{n}{r}Y_n(k_s r)\right) \quad 3.1.27$$

and

$$W_n(r)=-C_9^{(n)}\left(k_p J_{n+1}(k_p r)-\frac{n}{r}J_n(k_p r)\right)-C_{10}^{(n)}\left(k_p Y_{n+1}(k_p r)-\frac{n}{r}Y_n(k_p r)\right)$$
$$+C_{11}^{(n)}\frac{n}{r}J_n(k_s r)+C_{12}^{(n)}\frac{n}{r}Y_n(k_s r) \quad 3.1.28$$

where k_p is the plate wavenumber given by

$$k_p=\frac{\omega}{\sqrt{\frac{E}{\rho(1-\nu^2)}}} \quad 3.1.29$$

and k_s is the shear wavenumber given by

$$k_s=\frac{\omega}{\sqrt{\frac{E}{2\rho(1+\nu)}}} \quad 3.1.30$$

In equations 3.1.27 and 3.1.28, $C_j^{(n)}$ are unknown wave propagation coefficients, J_n is the n^{th} order Bessel function of the first kind and Y_n is the n^{th} order Bessel function of the second kind. Note that the index of the coefficients $C_j^{(n)}$ start at 9 as the coefficients for the shell end at 8. Also note

that for Bessel functions of the second kind, $\lim_{x\to 0} Y_n(x) = -\infty$. Therefore, $C_{10}^{(n)} = C_{12}^{(n)} = 0$ for all n in equations 3.1.27 and 3.1.28 as the displacement of the center of the plate ($r = 0$) must be finite. These equations reduce to

$$V_n(r) = -C_9^{(n)} \frac{n}{r} J_n(k_p r) + C_{10}^{(n)} \left(k_s J_{n+1}(k_s r) - \frac{n}{r} J_n(k_s r) \right) \tag{3.1.31}$$

and

$$W_n(r) = -C_9^{(n)} \left(k_p J_{n+1}(k_p r) - \frac{n}{r} J_n(k_p r) \right) + C_{10}^{(n)} \frac{n}{r} J_n(k_s r) \tag{3.1.32}$$

The out-of-plane motion of the plate is modeled using Kirchhoff-Love plate theory. The longitudinal equation of motion of the plate is given by Love [22] as

$$\begin{aligned} &\frac{\partial^4 u(r,\theta,t)}{\partial r^4} + \frac{2}{r}\frac{\partial^3 u(r,\theta,t)}{\partial r^3} - \frac{1}{r^2}\frac{\partial^2 u(r,\theta,t)}{\partial r^2} + \frac{1}{r^3}\frac{\partial u(r,\theta,t)}{\partial r} \\ &- \frac{2}{r^3}\frac{\partial^3 u(r,\theta,t)}{\partial r \partial \theta^2} + \frac{2}{r^2}\frac{\partial^4 u(r,\theta,t)}{\partial r^2 \partial \theta^2} + \frac{4}{r^4}\frac{\partial^2 u(r,\theta,t)}{\partial \theta^2} \\ &+ \frac{1}{r^4}\frac{\partial^4 u(r,\theta,t)}{\partial \theta^4} = -\frac{b\rho}{D_p}\frac{\partial^2 u(r,\theta,t)}{\partial t^2} \end{aligned} \tag{3.1.33}$$

where $u(r,\theta,t)$ is the longitudinal displacement of the plate, b is the thickness of the plate, and D_p is the flexural rigidity of the plate given by

$$D_p = \frac{Eb^3}{12(1-\nu^2)} \tag{3.1.34}$$

The solution to equation 3.1.33 has also been derived by Love [22] and is given as

$$u(r,\theta,t) = \sum_{n=0}^{\infty} U_n(r) \sin(n\theta) \exp(-i\omega t) \tag{3.1.35}$$

where

$$U_n(r) = C_{11}^{(n)} J_n(\zeta r) + C_{12}^{(n)} Y_n(\zeta r) + C_{13}^{(n)} I_n(\zeta r) + C_{14}^{(n)} K_n(\zeta r) \tag{3.1.36}$$

with

$$\zeta = \left(\frac{\omega^2 \rho b}{D_p} \right)^{\frac{1}{4}} \tag{3.1.37}$$

In equation 3.1.36, I_n is the modified Bessel function of the first kind, and K_n is the modified Bessel function of the second kind. Similar to Bessel functions of the second kind, $\lim_{x\to 0} K_n(x) = -\infty$. Equation 3.1.36 reduces to

$$U_n(r) = C_{11}^{(n)} J_n(\zeta r) + C_{12}^{(n)} I_n(\zeta r) \tag{3.1.38}$$

Since there are two plates in the system, the plate located at the left end of the shell will use the unknown wave propagation coefficient indexes 9 – 12, and the plate located at the right end of the shell will use the coefficient indexes 13 – 16.

As with the shell, the boundary equations used to solve for the unknown wave propagation coefficients require generalized forces and generalized moments found by integrating the stresses of an element of the plate over the thickness of the plate. The generalized forces corresponding to the in-plane stresses of the plate have been derived by Love [22] and are calculated in the tangential direction as

$$T_{r\theta}^{(n)}(r,\theta,t) = G\frac{\partial v(r,\theta,t)}{\partial r} - \frac{G}{r}v(r,\theta,t) + \frac{G}{r}\frac{\partial w(r,\theta,t)}{\partial \theta} \tag{3.1.39}$$

and in the radial direction as

$$T_{rr}^{(n)}(r,\theta,t) = \frac{E\nu}{1-\nu^2}\frac{1}{r}\frac{\partial v(r,\theta,t)}{\partial \theta} + \frac{E}{1-\nu^2}\frac{\partial w(r,\theta,t)}{\partial r} + \frac{E\nu}{1-\nu^2}\frac{1}{r}w(r,\theta,t) \tag{3.1.40}$$

where G is the bulk modulus. Leissa [23] derived the generalized shear force and moment corresponding to Kirchhoff-Love theory as

$$\begin{aligned} V_r(r,\theta,t) = -D_p\Bigg(&\frac{\partial^3 u(r,\theta,t)}{\partial r^3} + \frac{1}{r}\frac{\partial^2 u(r,\theta,t)}{\partial r^2} - \frac{1}{r^2}\frac{\partial u(r,\theta,t)}{\partial r} \\ &+ \frac{2-\nu}{r^2}\frac{\partial^3 u(r,\theta,t)}{\partial \theta^2 \partial r} - \frac{3-\nu}{r^3}\frac{\partial^2 u(r,\theta,t)}{\partial \theta^2}\Bigg) \end{aligned} \tag{3.1.41}$$

and

$$M_r(r,\theta,t) = -D_p\left(\frac{\partial^2 u(r,\theta,t)}{\partial r^2} + \frac{\nu}{r}\frac{\partial u(r,\theta,t)}{\partial r} + \frac{\nu}{r^2}\frac{\partial^2 u(r,\theta,t)}{\partial \theta^2}\right) \tag{3.1.42}$$

Section 3.1.3 will combine these generalized forces with the generalized forces from section 3.1.1 to form the boundary conditions of the system.

3.1.3 Boundary Conditions and Continuity Equations

From the above sections, there are 16 unknown coefficients to solve for. An equivalent number of boundary conditions are necessary to solve for them. Figure 3.1.2 shows the internal forces of the plates and shell. For the intersection of the left end of the shell and its corresponding plate located at $r = a$ and $z = z_l$, there are 3 generalized force equilibrium conditions

$$-V_z(a,\theta,z_l,t) + T_{rr}(a,\theta,z_l,t) = 0 \tag{3.1.43}$$

$$-V_\theta(a,\theta,z_l,t) + T_{r\theta}(a,\theta,z_l,t) = 0 \tag{3.1.44}$$

$$-N_z(a,\theta,z_l,t) + V_r(a,\theta,z_l,t) = 0 \tag{3.1.45}$$

and a generalized moment equilibrium

$$-M_z(a,\theta,z_l,t) + M_r(a,\theta,z_l,t) = 0 \tag{3.1.46}$$

There are also 3 displacement continuity equations

$$u_s(a,\theta,z_l,t) = u_{pl}(a,\theta,z_l,t) \tag{3.1.47}$$

$$v_s(a,\theta,z_l,t) = v_{pl}(a,\theta,z_l,t) \tag{3.1.48}$$

$$w_s(a,\theta,z_l,t) = w_{pl}(a,\theta,z_l,t) \tag{3.1.49}$$

and a slope continuity equation which maintains the right angle geometry of the connection between the plate and shell

$$\frac{\partial w_s(a,\theta,z_l,t)}{\partial z} = -\frac{\partial w_{pl}(a,\theta,z_l,t)}{\partial r} \tag{3.1.50}$$

Furthermore, there are 8 corresponding boundary conditions between the shell and the plate located at the right end of the shell $z = z_r$. These equations are

$$V_z(a,\theta,z_r,t) + T_{rr}(a,\theta,z_r,t) = 0 \tag{3.1.51}$$

$$V_\theta(a,\theta,z_r,t) + T_{r\theta}(a,\theta,z_r,t) = 0 \tag{3.1.52}$$

$$N_z(a,\theta,z_r,t) + V_r(a,\theta,z_r,t) = 0 \tag{3.1.53}$$

$$M_z(a,\theta,z_r,t) + M_r(a,\theta,z_r,t) = 0 \tag{3.1.54}$$

$$u_s(a,\theta,z_r,t) = u_{pr}(a,\theta,z_r,t) \tag{3.1.55}$$

$$v_s(a,\theta,z_r,t) = v_{pr}(a,\theta,z_r,t) \tag{3.1.56}$$

$$w_s(a,\theta,z_r,t) = w_{pr}(a,\theta,z_r,t) \tag{3.1.57}$$

$$\frac{\partial w_s(a,\theta,z_r,t)}{\partial z} = -\frac{\partial w_{pr}(a,\theta,z_r,t)}{\partial r} \tag{3.1.58}$$

The expressions for the forces and displacements of the shell and plates are input into equations 3.1.43 – 3.1.58. The resulting equations have infinite summations of circumferential modes in each term. These circumferential modes can be decoupled into an infinite set of indexed equations via the orthogonalization method mentioned in section 3.1.1.

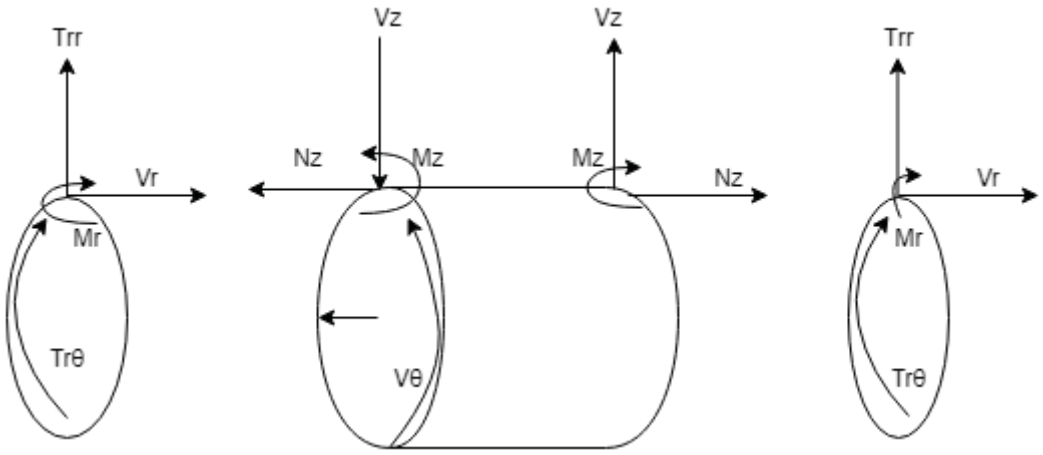

Figure 3.1.2 – Free body diagram of the system

The orthogonalization of equations 3.1.43 – 3.1.58 yields an infinite set of 16 n-indexed boundary conditions. Each set of boundary conditions can be written in a matrix form

$$\boldsymbol{A}_n \boldsymbol{x}_n = \boldsymbol{b}_n \tag{3.1.59}$$

where the entries of the square matrix $\boldsymbol{A}_n$ are in Appendix A, the vector $\boldsymbol{x}_n$ contains the unknown wave propagation coefficients and is given by

$$\boldsymbol{x}_n = \left\{C_1^{(n)}, C_2^{(n)}, \dots, C_{16}^{(n)}\right\} \tag{31.60}$$

and the vector $\boldsymbol{b}_n$ contains the excitation terms and is given by

$$\boldsymbol{b}_n = \{0, \dots, 0\} \tag{3.1.61}$$

as the system currently has no external forces applied to it. The wave propagation coefficients for each index are solved for by

$$\boldsymbol{x}_n = \boldsymbol{A}_n^{-1} \boldsymbol{b}_n \tag{3.1.62}$$

The wave propagation coefficient solutions can be entered into 3.1.5 – 3.1.7, 3.1.25, 3.1.26, and 3.1.35 to compute the displacement field solutions for the shell and plates. With $\boldsymbol{b}_n$ currently being the zero vector, equation 3.1.62 will only result in entirely zero wave propagation coefficients. Similar to solving for the eigenvalues of the shell in section 3.1.1, the determinant of $\boldsymbol{A}_n$ gives the natural frequencies of the system. The following sections discussing the types of excitations applied to the system will adjust the values in the $\boldsymbol{b}_n$ vector resulting in nonzero displacement field solutions.

3.2 Application of the Ring Load

3.2.1 Generalized Forces Due to Ring Loads

As mentioned in Chapter 2, the ring load is a pressure given by

$$P(r,\theta,z,t) = P_0 e^{ikz} e^{-i\omega t} \tag{3.2.1}$$

where P_0 is the constant pressure magnitude, k is the excitation wavenumber, and ω is the excitation frequency. This loading condition consists of a radial pressure wave on the outer surface of the shell that propagates about the shell's longitudinal axis. Therefore, this excitation must be included in the radial generalized force boundary conditions 3.1.43 and 3.1.51. Figure 3.2.1 shows an element of the shell and the forces acting in the radial direction. As the longitudinal span dx approaches zero, the sum of forces in the radial direction reduces to

$$\sigma_{\theta r} dS_\theta dr = P dS_\theta$$

Note that, as mentioned in section 3.1.1, the generalized forces due to the internal stresses of the system are calculated by integrating the stress over the thickness of the shell. In thin shell theory, external loadings are applied after the shell has been reduced to a middle surface. Therefore, the external load term is a constant integrated over the thickness of the shell and becomes the generalized force $PhdS_\theta$. The dS_θ term is canceled across the equation, and the external load term that is entered into the boundary conditions is simply $P(r,\theta,z,t)h$.

The force balances in equations 3.1.43 and 3.1.51 now become

$$-V_z(a,\theta,z_l,t) + T_{rr}(a,\theta,z_l,t) + P(a,\theta,z_l,t)h = 0 \tag{3.2.2}$$

$$V_z(a,\theta,z_r,t) + T_{rr}(a,\theta,z_r,t) + P(a,\theta,z_r,t)h = 0 \tag{3.2.3}$$

The appropriate expressions are substituted into the equations, the temporal component $e^{-i\omega t}$ in each term is canceled, and the equations are rearranged into the form

$$\big(-V_z(a,\theta,z_l,t) + T_{rr}(a,\theta,z_l,t)\big)e^{i\omega t} = -P_0 e^{ikz_l} h \tag{3.2.4}$$

$$\big(-V_z(a,\theta,z_l,t) + T_{rr}(a,\theta,z_l,t)\big)e^{i\omega t} = -P_0 e^{ikz_r} h \tag{3.2.5}$$

where the expressions for the internal forces of the shell and plate are not shown for visual clarity. The boundary conditions are orthogonalized about θ. Since the ring load terms do not contain θ, they are orthogonalized as

$$\int_0^{2\pi} -P_0 e^{ikz} h \cos n_2\theta \, d\theta = -P_0 e^{ikz} h \int_0^{2\pi} \cos n_2\theta \, d\theta = -P_0 e^{ikz} h \delta_{n_0}$$

where δ_{n_0} is the Dirac delta function. The ring load only excites the $n = 0$ circumferential modes of the system. The ring load terms on the right hand side of the above equations enter equation 3.1.59 in their respective locations within the force vector $\boldsymbol{b}$.

3.2.2 Generalized Moments Due to Ring Loads

The pressure is distributed across the shell which creates moments about the points where the moment boundary conditions are evaluated. The moment due to the excitation will be denoted by M_p. Similar to the force balances, the moment balances in equations 3.1.46 and 3.1.54 are generalized moments. The generalized moments due to external loads are found by integrating the generalized force over the range of the generalized force. In equation form, the generalized moment about the left end of the shell due to the ring load is given by

$$M_p(a,\theta,z_l,t) = \int_0^L P(a,\theta,z,t)hzdz = \frac{P_0 h}{(ik)^2}\Big((ikz-1)e^{ikz}\Big|_0^L$$
$$= \frac{P_0 h}{(ik)^2}e^{-i\omega t}\Big((ikL-1)e^{ikL}-1\Big) \qquad 3.2.6$$

The equilibrium equations 3.1.46 and 3.1.54 become

$$-M_z(a,\theta,z_l,t) + M_r(a,\theta,z_l,t) + M_p(a,\theta,z_l,t) = 0 \qquad 3.2.6$$

$$M_z(a,\theta,z_r,t) + M_r(a,\theta,z_r,t) - M_p(a,\theta,z_r,t) = 0 \qquad 3.2.7$$

This expression for the moment enters the moment boundary conditions 3.2.6 and 3.2.7. Rearranging the equations and canceling the temporal terms leads to

$$\big(-M_z(a,\theta,z_r,t) + M_r(a,\theta,z_r,t)\big)e^{i\omega t} = -\frac{P_0 h}{(ik)^2}\Big((ikL-1)e^{ikL}-1\Big) \qquad 3.2.8$$

$$\big(M_z(a,\theta,z_r,t) + M_r(a,\theta,z_r,t)\big)e^{i\omega t} = \frac{P_0 h}{(ik)^2}\Big((ikL-1)e^{ikL}-1\Big) \qquad 3.2.9$$

Orthogonalizing again leads to the moment due to the ring load only influencing the first circumferential mode.

$$\int_0^{2\pi} -\frac{P_0 h}{(ik)^2}\Big((ikL-1)e^{ikL}-1\Big)\cos n_2\theta\, d\theta = -\frac{P_0 h}{(ik)^2}\Big((ikL-1)e^{ikL}-1\Big)\delta_{n_0} \qquad 3.2.10$$

$$\int_0^{2\pi} \frac{P_0 h}{(ik)^2}\Big((ikL-1)e^{ikL}-1\Big)\cos n_2\theta\, d\theta = \frac{P_0 h}{(ik)^2}\Big((ikL-1)e^{ikL}-1\Big)\delta_{n_0} \qquad 3.2.11$$

The terms on the right hand side of the above equations enter 3.1.59 in their respective locations within the force vector $\boldsymbol{b}$. The $\boldsymbol{A}$ matrix determined in section 3.1 can now be inverted and post multiplied by $\boldsymbol{b}$ to solve for the unknown wave propagation coefficients. Since the ring load only

excites the zeroth mode, the displacement field solutions will converge with only the zeroth mode included in the solution.

3.3 Derivation of the Plane Wave Excitation

The plane wave in Cartesian coordinates as stated in Chapter 2 is given by

$$P_i(x, y, z, t) = P_0 e^{i(\boldsymbol{kr} - \omega t)} \tag{3.3.1}$$

where P_0 is the constant pressure magnitude, $\boldsymbol{r} = [x, y, z]^T$ is the location vector of the wave, $\boldsymbol{k} = \left[k_x, k_y, k_z\right]^T$ is the vector of excitation wavenumber components in each direction, and ω is the excitation frequency. This equation can be expanded to

$$P_i(x, y, z, t) = P_0 e^{i(\boldsymbol{kr} - \omega t)} = P_0 e^{ik_x x} e^{ik_y y} e^{ik_z z} e^{-i\omega t} \tag{3.3.2}$$

Since the shell is symmetric about the longitudinal axis, the range of possible plane waves can be reduced to only those propagating in the x-z plane which corresponds to the r-z plane when $\theta = 0$ in cylindrical coordinates. The wavenumber vector is reduced to $\boldsymbol{k} = [k_x, 0, k_z]^T$. Given any angle of incidence ϕ_i of the plane wave as shown in Figure 3.3.1, the wavenumber vector becomes $\boldsymbol{k} = [k \cos \phi_i\,, 0, k \sin \phi_i]^T$ where k is the excitation wavenumber of the plane wave along the axis it propagates. In this study, the excitation wavenumber will be linked to the properties of the fluid it propagates in as

$$k = \frac{\omega}{c_f} \tag{3.3.3}$$

where c_f is the wave speed of the fluid.

It is clear from the Figure 3.3.1 that the case where $\pi \leq \phi_i \leq 2\pi$ is equivalent to the negative of the case where $0 \leq \phi_i \leq \pi$. It is also clear from the figure that the case where $\frac{\pi}{2} \leq \phi_i \leq \pi$ is a mirror image of the case where $0 \leq \phi_i \leq \frac{\pi}{2}$. Therefore, ϕ_i can be restricted to the range $0 \leq \phi_i \leq \frac{\pi}{2}$ without a loss of generality. This range leaves two special cases of the plane wave: one where $\phi_i = 0$ henceforth known as the broadside plane wave, and one where $\phi_i = \frac{\pi}{2}$ henceforth known as the frontside plane wave.

The plane wave must be converted to cylindrical coordinates to be used in the model. The relation between Cartesian coordinates and cylindrical coordinates are as follows:

$$x = r \cos \theta\,, \quad y = r \sin \theta\,, \quad z = z \tag{3.3.4}$$

Since all cases of $\theta \neq 0$ have been eliminated due to symmetry, the equation for the plane wave in cylindrical coordinates is then

$$P_i(r,\theta,z,t) = P_0 e^{ik_r r\cos\phi_i} e^{ik_z z} e^{-i\omega t} \tag{3.3.5}$$

where $k_r = k_x = k\cos\phi_i$. The term $e^{ik_r r\cos\phi_i}$ can be rewritten using the Jacobi-Anger expansion as

$$e^{ik_r r\cos\phi_i} = J_0(k_r r) + 2\sum_{n=1}^{\infty} i^n J_n(k_r r)\cos(n\theta) \tag{3.3.6}$$

where J_n is the Bessel function of the first kind. This expression can be condensed to

$$e^{ik_r r\cos\phi_i} = \sum_{n=1}^{\infty} \varepsilon_n i^n J_n(k_r r)\cos(n\theta) \tag{3.3.7}$$

where

$$\varepsilon_n = \begin{cases} 1, & n = 0 \\ 2, & n > 0 \end{cases} \tag{3.3.8}$$

Therefore, the cylindrical coordinate form of the plane wave is

$$P_i(r,\theta,z,t) = P_0 e^{ik_z z} e^{-i\omega t} \sum_{n=0}^{\infty} \varepsilon_n i^n J_n(k_r r)\cos(n\theta) \tag{3.3.9}$$

Similar to the assumed solution of the displacement of the model, this form of the plane wave contains an infinite series of circumferential modes.

3.4 Broadside Plane Waves

3.4.1 Generalized Forces Due to Broadside Plane Waves

Broadside plane waves are a special case of the plane wave where the angle of incidence of the wave has the value $\phi_i = 0$. The wavenumber components become $k_r = k\cos\phi_i = k$ and $k_z = k\sin\phi_i = 0$. Equation 3.3.9 is reduced to

$$P_i(r,\theta,z,t) = P_0 e^{-i\omega t} \sum_{n=0}^{\infty} \varepsilon_n i^n J_n(kr)\cos(n\theta) \tag{3.4.1}$$

Since the broadside plane wave propagates perpendicular to the longitudinal axis, the force in 3.3.8 is included only in the radial force boundary conditions 3.1.43 and 3.1.51. Like the ring load, the

generalized force term due to the broadside plane wave is $P_i(r,\theta,z,t)h$. The force balances now become

$$-V_z(a,\theta,z_l,t) + T_{rr}(a,\theta,z_l,t) - P_i(a,\theta,z_l,t)h = 0 \tag{3.4.2}$$

$$V_z(a,\theta,z_r,t) + T_{rr}(a,\theta,z_r,t) - P_i(a,\theta,z_r,t)h = 0 \tag{3.4.3}$$

The temporal component $e^{-i\omega t}$ in each term is canceled, and the boundary conditions are rearranged into the form

$$\big(-V_z(a,\theta,z_l,t) + T_{rr}(a,\theta,z_l,t)\big)e^{i\omega t} = P_0 h \sum_{n=0}^{\infty} \varepsilon_n i^n J_n(ka)\cos(n\theta) \tag{3.4.4}$$

$$\big(V_z(a,\theta,z_l,t) + T_{rr}(a,\theta,z_l,t)\big)e^{i\omega t} = P_0 h \sum_{n=0}^{\infty} \varepsilon_n i^n J_n(ka)\cos(n\theta) \tag{3.4.5}$$

where the expressions for the internal forces of the shell and plate are not shown for visual clarity. The equations are orthogonalized about θ resulting in the mode decoupled form

$$\int_0^{2\pi} P_0 h \sum_{n=0}^{\infty} \varepsilon_n i^n J_n(ka)\cos(n\theta)\cos(n_2\theta)\,d\theta = P_0 h \varepsilon_n i^n J_n(ka) \tag{3.4.6}$$

The broadside plane wave term on the right hand side of the above equation enters equation 3.1.59 in its appropriate locations within the force vector $\boldsymbol{b}$.

3.4.2 Generalized Moments Due to Broadside Plane Waves

The moments caused by the broadside plane wave can be solved for in a similar fashion to the ring load. Once again, the generalized moment is found by integrating the generalized force over the range of the generalized force. For broadside plane waves, the generalized moment is

$$M_p(a,\theta,z_l,t) = \int_0^L P_i(a,\theta,z,t)h\,z\,dz = \int_0^L P_0 h e^{-i\omega t} \sum_{n=0}^{\infty} \varepsilon_n i^n J_n(ka)\cos(n\theta)\,z\,dz$$

$$= P_0 h e^{-i\omega t} \sum_{n=0}^{\infty} \varepsilon_n i^n J_n(ka)\cos(n\theta) \int_0^L z dz = \frac{P_0 h L^2}{2} e^{-i\omega t} \sum_{n=0}^{\infty} \varepsilon_n i^n J_n(ka)\cos(n\theta) \tag{3.4.9}$$

This expression is now entered into the generalized moment equilibrium equations

$$-M_z(a,\theta,z_l,t) + M_r(a,\theta,z_l,t) - M_p(a,\theta,z_l,t) = 0 \tag{3.4.8}$$

$$M_z(a,\theta,z_r,t) + M_r(a,\theta,z_r,t) + M_p(a,\theta,z_r,t) = 0 \tag{3.4.9}$$

Rearranging equations 3.4.8 and 3.4.9, entering the expressions for the moments, and canceling the temporal term results in

$$\left(-M_z(a,\theta,z_l,t)+M_r(a,\theta,z_l,t)\right)e^{i\omega t}=\frac{P_0hL^2}{2}\sum_{n=0}^{\infty}\varepsilon_n i^n J_n(ka)\cos(n\theta) \qquad 3.4.11$$

$$\left(M_z(a,\theta,z_l,t)+M_r(a,\theta,z_l,t)\right)e^{i\omega t}=-\frac{P_0hL^2}{2}\sum_{n=0}^{\infty}\varepsilon_n i^n J_n(ka)\cos(n\theta) \qquad 3.4.12$$

Orthogonalizing these equations about θ results in the mode decoupled moment boundary conditions

$$\int_0^{2\pi}\frac{P_0hL^2}{2}\sum_{n=0}^{\infty}\varepsilon_n i^n J_n(ka)\cos(n\theta)\cos(n_2\theta)\,d\theta=\frac{P_0hL^2}{2}\varepsilon_n i^n J_n(ka) \qquad 3.4.13$$

$$\int_0^{2\pi}-\frac{P_0hL^2}{2}\sum_{n=0}^{\infty}\varepsilon_n i^n J_n(ka)\cos(n\theta)\cos(n_2\theta)\,d\theta=-\frac{P_0hL^2}{2}\varepsilon_n i^n J_n(ka) \qquad 3.4.14$$

Terms on the right side of the above equations enter 3.1.59 in their respective locations within the force vector $\boldsymbol{b}$. The model is now prepared to calculate the unknown wave propagation coefficients for a broadside plane wave.

It is important to note that, unlike the ring load, broadside plane waves are not symmetric about the longitudinal axis. Waves of this type excite all of the circumferential modes; therefore, there will be circumferential displacements present in the system. Another dissimilarity to the ring load is nonzero wave propagation solutions for nonzero circumferential modes. In order for the displacement field solutions from the model to converge, a number of modes will need to be included in the solution. Since the model solves the decoupled mode equations sequentially, the computation time for a broadside plane wave may be much longer than that of the ring load.

3.5 Frontside Plane Waves

3.5.1 Generalized Forces Due to Frontside Plane Waves

Frontside plane waves are the other special case of the plane wave where the wave's angle of incidence is $\phi_i=\frac{\pi}{2}$. The wavenumber components in this case reduce to $k_r=0$ and $k_z=k$. Using equation 3.3.7, the frontside plane wave is given by

$$P_i(r,\theta,z,t)=P_0e^{ik_zz}e^{-i\omega t} \qquad 3.5.1$$

since $J_n(0) = 0$. Unlike ring loads and broadside plane waves, frontside plane waves are longitudinal pressure waves. They act on the endcaps in this system. The generalized forces on the endcaps are found the same way as the generalized forces on the shell. However, the forces are integrated over the width of the plates. The generalized force of a frontside plane wave is then given by $P_i(r, \theta, z, t)b$. Therefore, the longitudinal force balances must be adjusted to include the force described in 3.5.1. These boundary conditions become

$$-V_r(a, \theta, z_l, t) + N_z(a, \theta, z_l, t) + P_i(a, \theta, z_l, t)b = 0 \tag{3.5.2}$$

$$V_r(a, \theta, z_r, t) + N_z(a, \theta, z_r, t) + P_i(a, \theta, z_r, t)b = 0 \tag{3.5.3}$$

Inputting the relevant expressions, rearranging these equations results, and canceling the temporal term results in

$$\left(-V_r(a, \theta, z_r, t) + N_z(a, \theta, z_r, t)\right)e^{-i\omega t} = -P_0 e^{ik_z z} b \tag{3.5.4}$$

$$\left(V_r(a, \theta, z_r, t) + N_z(a, \theta, z_r, t)\right)e^{-i\omega t} = -P_0 e^{ik_z z} b \tag{3.5.5}$$

where the expressions for the internal forces of the shell and plate are not shown for visual clarity. As with the ring load, the orthogonalization of the above equations results in

$$\int_0^{2\pi} -P_0 e^{ik_z z} b \cos(n_2 \theta)\, d\theta = -P_0 e^{ik_z z} b \delta_{n_0} \tag{3.5.6}$$

where the frontside plane wave terms only appear in the zeroth circumferential mode. This is similar to the ring loading in section 3.2 as both the ring load and frontside plate wave are symmetric about the longitudinal axis. The term on the right side of the equality in 3.5.6 enter 3.1.59 in its respective locations in the vector $\boldsymbol{b}$.

3.5.2 Generalized Moments Due to Frontside Plane Waves

The generalized moments caused by the frontside plane wave are calculated by integrating the generalized force as

$$M_p(a, \theta, z_l, t) = \int_0^a P_i(a, \theta, z, t) b\, r\, dr = P_i(a, \theta, z, t) b \frac{a^2}{2} \tag{3.5.7}$$

Note the limits of integration do not span the diameter of the plate as the radial dimension in cylindrical coordinates has the range $r \in [0, \infty)$. The generalized moments appear in the usual moment boundary conditions as

$$-M_z(a, \theta, z_l, t) + M_r(a, \theta, z_l, t) + M_p(a, \theta, z_l, t) = 0 \tag{3.5.8}$$

$$M_z(a, \theta, z_r, t) + M_r(a, \theta, z_r, t) + M_p(a, \theta, z_r, t) = 0 \tag{3.5.9}$$

Substituting this expression into 3.5.8 and 3.5.9, rearranging, and canceling the temporal term results in the mode decoupled boundary conditions

$$\left(-M_z(a,\theta,z_l,t)+M_r(a,\theta,z_l,t)\right)e^{i\omega t}=-\frac{a^2P_0}{2}e^{ik_zz} \tag{3.5.10}$$

$$\left(M_z(a,\theta,z_l,t)+M_r(a,\theta,z_l,t)\right)e^{i\omega t}=-\frac{a^2P_0}{2}e^{ik_zz} \tag{3.5.11}$$

Orthogonalizing the above equations results in the decoupled moment term

$$\int_0^{2\pi}-\frac{a^2P_0}{2}e^{ik_zz}\cos(n_2\theta)\,d\theta=-\frac{a^2P_0}{2}e^{ik_zz}\delta_n \tag{3.5.12}$$

where the frontside plane equations only excite the zeroth circumferential mode as they are symmetric about the longitudinal axis. The plane wave term above enters 3.1.59 in its respective locations in $\boldsymbol{b}$, and the model is now ready to evaluate the unknown wave propagation coefficients due to the frontside plane wave excitation. As with the ring load, only the zeroth mode is required for the solution to converge.

3.6 General Plane Waves

3.6.1 Generalized Forces Due to General Plane Waves

As derived earlier, the general case of the plane wave with $\phi_i \in \left(0,\frac{\pi}{2}\right)$ is given by

$$P_i(r,\theta,z,t)=P_0e^{ik_zz}e^{-i\omega t}\sum_{n=0}^{\infty}\varepsilon_n i^nJ_n(k_rr)\cos(n\theta) \tag{3.6.1}$$

Both the shell and plates are excited. In order to properly apply this excitation to the system, the force balances in both the radial and longitudinal directions must be altered. Despite the complex nature of equation 3.6.1, the forces applied to both the shell and the plate are constant across the thickness of the shell and plate, respectively. The generalized force applied to the shell is given by $P_i(r,\theta,z,t)h$, and the generalized force applied to the plates is given by $P_i(r,\theta,z,t)b$. The radial force balances are now

$$-V_z(a,\theta,z_l,t)+T_{rr}(a,\theta,z_l,t)-P_i(a,\theta,z_l,t)h=0 \tag{3.6.2}$$

$$V_z(a,\theta,z_r,t)+T_{rr}(a,\theta,z_r,t)-P_i(a,\theta,z_r,t)h=0 \tag{3.6.3}$$

and the longitudinal forces balances are

$$-V_r(a,\theta,z_l,t)+N_z(a,\theta,z_l,t)+P_i(a,\theta,z_l,t)b=0 \tag{3.6.4}$$

$$V_r(a,\theta,z_r,t)+N_z(a,\theta,z_r,t)+P_i(a,\theta,z_r,t)b=0 \tag{3.6.5}$$

Rearranging the equations, substituting the proper expressions, and removing the temporal term results in the radial force balances

$$\left(-V_z(a,\theta,z_r,t)+T_{rr}(a,\theta,z_r,t)\right)e^{i\omega t}=P_0 h e^{ik_z z_l}\sum_{n=0}^{\infty}\varepsilon_n i^n J_n(k_r a)\cos(n\theta) \qquad 3.6.6$$

$$\left(V_z(a,\theta,z_r,t)+T_{rr}(a,\theta,z_r,t)\right)e^{i\omega t}=P_0 h e^{ik_z z_r}\sum_{n=0}^{\infty}\varepsilon_n i^n J_n(k_r a)\cos(n\theta) \qquad 3.6.7$$

and the longitudinal force balances

$$\left(-V_r(a,\theta,z_r,t)+N_z(a,\theta,z_r,t)\right)e^{i\omega t}=-P_0 b e^{ik_z z_l}\sum_{n=0}^{\infty}\varepsilon_n i^n J_n(k_r a)\cos(n\theta) \qquad 3.6.8$$

$$\left(V_r(a,\theta,z_r,t)+N_z(a,\theta,z_r,t)\right)e^{i\omega t}=-P_0 b e^{ik_z z_r}\sum_{n=0}^{\infty}\varepsilon_n i^n J_n(k_r a)\cos(n\theta) \qquad 3.6.9$$

Orthogonalizing the above equations results in the mode decoupled external radial force term

$$\int_0^{2\pi} P_0 h e^{ik_z z_l}\sum_{n=0}^{\infty}\varepsilon_n i^n J_n(k_r a)\cos(n\theta)\cos(n_2\theta)\,d\theta=P_0 h e^{ik_z z_l}\varepsilon_n i^n J_n(k_r a) \qquad 3.6.10$$

and mode decoupled external longitudinal force term

$$\int_0^{2\pi} -P_0 b e^{ik_z z_l}\sum_{n=0}^{\infty}\varepsilon_n i^n J_n(k_r a)\cos(n\theta)\cos(n_2\theta)\,d\theta=-P_0 b e^{ik_z z_l}\varepsilon_n i^n J_n(k_r a) \qquad 3.6.11$$

The right hand sides of equations 3.6.10 and 3.6.11 enter the $\boldsymbol{b}$ vector in equation 3.1.59 in their respective locations.

3.6.2 Generalized Moments Due to General Plane Waves

Since a plane wave approaching at an angle of incidence $\phi_i \in \left(0,\frac{\pi}{2}\right)$ excites the shell and both plates, two moment terms will need to added to each of the moment balances in equations 3.1.46 and 3.1.54. Moments due to the wave acting on the shell will be denoted M_s, and moments due to the wave acting on the plates will be denoted M_p. As in sections 3.4 and 3.5, M_s is given as

$$M_s = \int_0^L P_0 h e^{ik_z z} e^{-i\omega t} \sum_{n=0}^{\infty} \varepsilon_n i^n J_n(k_r a)\cos(n\theta)\, z dz$$

$$= P_0 h e^{-i\omega t} \sum_{n=0}^{\infty} \varepsilon_n i^n J_n(k_r a)\cos(n\theta) \int_{z_l}^{z_r} z e^{ik_z z}\, dz$$

$$= \frac{P_0 h e^{-i\omega t}}{(ik)^2}\left((ikL-1)e^{ikL}-1\right)\sum_{n=0}^{\infty} \varepsilon_n i^n J_n(k_r a)\cos(n\theta) \qquad 3.6.12$$

and M_p is given by

$$M_p = \int_0^r P_0 b e^{ik_z z} e^{-i\omega t} \sum_{n=0}^{\infty} \varepsilon_n i^n J_n(k_r r)\cos(n\theta)\, r dr$$

$$= P_0 b e^{ik_z z} e^{-i\omega t} \int_0^r \sum_{n=0}^{\infty} \varepsilon_n i^n J_n(k_r r)\cos(n\theta)\, r dr \qquad 3.6.13$$

The sum rule in integration allows the summation and integral to be swapped resulting in

$$M_p = P_0 b e^{ik_z z} e^{-i\omega t} \sum_{n=0}^{\infty} \varepsilon_n i^n \left[\int_0^a r J_n(k_r r) dr\right]\cos(n\theta) \qquad 3.6.14$$

In order to compute the integral of a Bessel function, the order of the Bessel function must be considered. For zeroth order Bessel functions, the integral expression in 3.6.19 evaluates to

$$\int_0^a r J_0(k_r r) dr = (r J_1(k_r r)|_0^a = a J_1(k_r a) \qquad 3.6.15$$

For Bessel functions of order $n > 1$, the integral term in 3.6.19 is given by

$$\int_0^a r J_n(k_r r) dr$$

$$= \left(2^{-n-1} r^2 (k_r r)^n \Gamma\left(\frac{n}{2}+1\right) {}_1\tilde{F}_2\left(\frac{n}{2}+1; n+1, \frac{n}{2}+2; -\frac{1}{4}k_r^2 r^2\right)\right|_0^a$$

$$= 2^{-n-1} a^2 (k_r a)^n \Gamma\left(\frac{n}{2}+1\right) {}_1\tilde{F}_2\left(\frac{n}{2}+1; n+1, \frac{n}{2}+2; -\frac{1}{4}k_r^2 a^2\right) \qquad 3.6.16$$

where the Euler gamma function Γ is an extension of the factorial

$$\Gamma(x) = (x-1)!$$

where ${}_1\tilde{F}_2$ is the regularized generalized hypergeometric function given by

$$ {}_p\tilde{F}_q\left(a_1,\dots,a_p;b_1,\dots,b_q;z\right)=\sum_{k=0}^{\infty}\frac{\prod_{j=1}^{p}\left(a_j\right)_k z^k}{k!\prod_{j=1}^{q}\Gamma\left(k+b_j\right)} \tag{3.6.17}$$

Generalized hypergeometric functions are power series where the ratio of k-indexed coefficients forms a rational function of k.

The generalized moment boundary conditions become

$$-M_z(a,\theta,z_l,t)+M_r(a,\theta,z_l,t)-M_s(a,\theta,z_l,t)+M_p(a,\theta,z_l,t)=0 \tag{3.6.18}$$

$$M_z(a,\theta,z_r,t)+M_r(a,\theta,z_r,t)+M_s(a,\theta,z_l,t)+M_p(a,\theta,z_r,t)=0 \tag{3.6.19}$$

Rearranging these equations, substituting the appropriate expressions, canceling the temporal term, and orthogonalizing the equations about θ results in decoupled moment equations for the zeroth mode

$$\begin{aligned}\int_0^{2\pi}\Big(M_s(a,\theta,z_l,t)-M_p(a,\theta,z_l,t)\Big)\cos(n_2\theta)\,d\theta=\\ \frac{P_0h}{(ik_z)^2}\Big((ik_zL-1)e^{ik_zL}-1\Big)\varepsilon_{\mathrm{n}}i^nJ_n(k_ra)\\ -P_0be^{ik_zz_l}\varepsilon_{\mathrm{n}}i^n\left(2^{-n-1}a^2(k_ra)^n\Gamma\left(\frac{n}{2}+\frac{1}{2}\right){}_1\tilde{F}_2\left(\frac{n}{2}+\frac{1}{2};n+1,\frac{n}{2}+\frac{3}{2};-\frac{1}{4}k_r^2a^2\right)\right)\end{aligned} \tag{3.6.20}$$

$$\begin{aligned}\int_0^{2\pi}\Big(-M_s(a,\theta,z_r,t)-M_p(a,\theta,z_r,t)\Big)\cos(n_2\theta)\,d\theta=\\ \frac{P_0h}{(ik_z)^2}\Big((ik_zL-1)e^{ik_zL}-1\Big)\varepsilon_{\mathrm{n}}i^nJ_n(k_ra)\\ -P_0be^{ik_zz_r}\varepsilon_{\mathrm{n}}i^n\left(2^{-n-1}a^2(k_ra)^n\Gamma\left(\frac{n}{2}+\frac{1}{2}\right){}_1\tilde{F}_2\left(\frac{n}{2}+\frac{1}{2};n+1,\frac{n}{2}+\frac{3}{2};-\frac{1}{4}k_r^2a^2\right)\right)\end{aligned} \tag{3.6.21}$$

The right side of the above equations enter 3.1.59 in $\boldsymbol{b}$. The model is now capable of calculating displacement field solutions of the system due to any plane wave orientation.

Chapter 4
Model Results and Validation

This chapter begin with a discussion of the finite element model used to validate the results of the model in Chapter 3. The remaining sections of this chapter will contain the validation of each excitation and discussion of the results due to each excitation.

4.1 Finite Element Model of the System

In order to verify the results of the model derived in Chapter 3, a Nastran finite element model was compared to the analytical model for each excitation. A CAD model of a shell and endcap system using the dimensions in Table 4.1.1 was created in Autodesk Inventor. Figure 4.1.1 displays the CAD model used for validation. The model was then imported into Nastran where it was meshed using quadrilateral shell elements as shown in Figure 4.1.2, and the loading conditions and simulation settings in Table 4.1.2 were applied.

Table 4.1.1 – Dimensions of the system

Parameter	Description	Value	Units
a	Radius of the shell and plates	2	m
L	Length of the shell	2	m
h	Thickness of the shell	0.001	m
b	Thickness of the plates	0.001	m

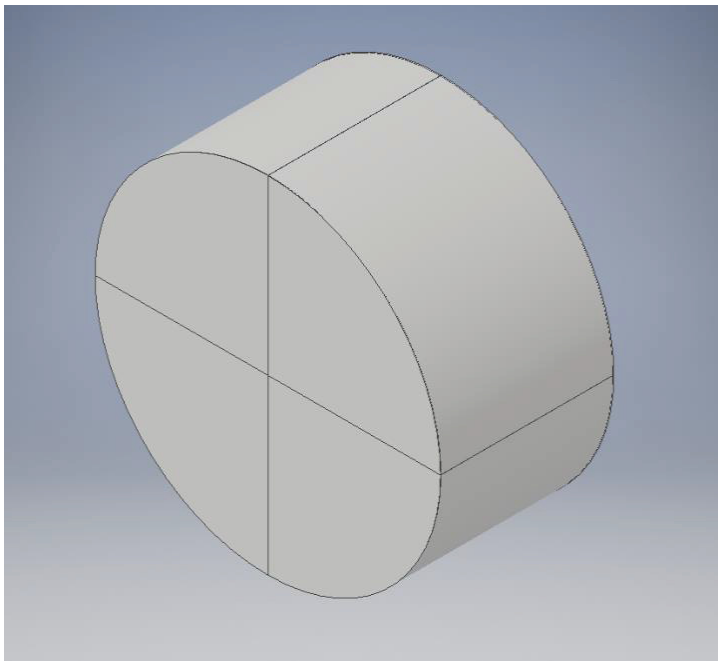

Figure 4.1.1 – CAD model of the validation shell

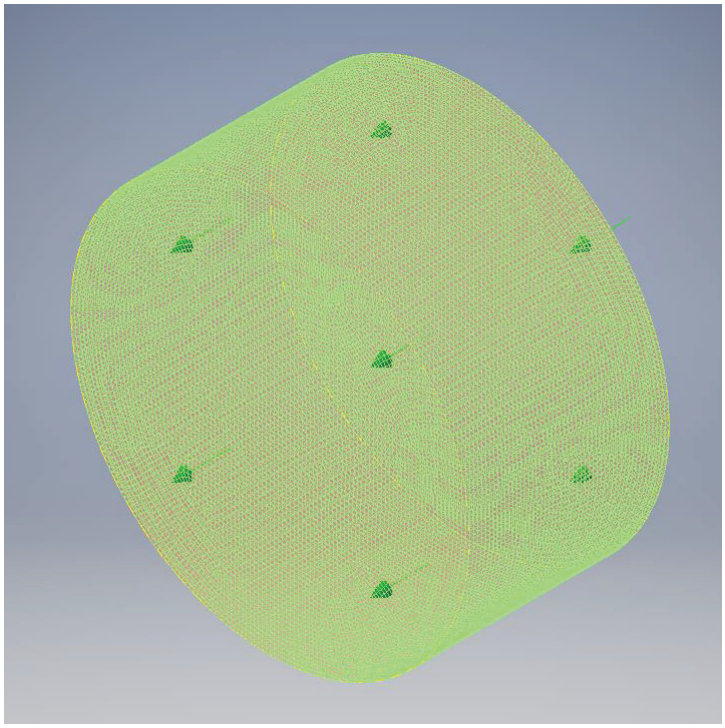

Figure 4.1.2 – Finite element model of CAD model in Figure 4.1.1

Table 4.1.2 – Finite element model settings

Parameter	Description	Value	Units
Analysis Type	Solution method used to solve the model	Modal Frequency Response	-
Eigenvalues	Number of eigenvalues used in the Modal Frequency Response method	50	-
Nodes	Total number of nodes	97322	-
Elements	Total number of elements	32440	-
Element Type	Elements used in the mesh in Figure 4.1.2	Parabolic Shell Elements	-
ρ	Material density	7800	kg/m^3
E	Elastic modulus	2.00E+11	Pa
ν	Poisson's Ratio	0.3	-
Damping	Structural damping value of the elements	0%	-
P_0	Excitation magnitude for all excitations	1	Pa
ω	Excitation frequency for all excitations	10	Hz
ϕ_i	Angle of approach for the general plane wave case	30	deg
θ	Circumferential angle for results	0	deg

The modal frequency response mentioned in Table 4.1.2 involves computing equivalent mass, damping, and stiffness matrices in the form

$$\boldsymbol{M}\ddot{\boldsymbol{x}}(t) + \boldsymbol{B}\dot{\boldsymbol{x}}(t) + \boldsymbol{K}\boldsymbol{x}(t) = \boldsymbol{P}(\omega)e^{i\omega t} \quad 4.1.1$$

Lanczos algorithm is used to extract the eigenvalues of the system up to a total number of eigenvalues defined by the user. Nastran then constructs nodal solutions in the form

$$x(t) = u(\omega)e^{i\omega t} \quad 4.1.2$$

These nodal solutions can then be queried individually, or over any defined line or surface. In the following sections, the displacement solutions are shown over the length of the shell for a specific circumferential angle θ.

4.2 Validation of the Ring Loading Condition

A comparison of the wave propagation model and the finite element model is shown in Figures 4.2.1 and 4.2.2. Table 4.2.1 shows the parameter values used in the wave propagation

method that have not been mentioned in either Table 4.1.1 or 4.1.2. The values in this table are used for all of the different excitations. Note the scale on the vertical axis of these plots is a decibel scale of the maximum displacement at each point. In the wave propagation model, this is equivalent to removing the temporal component of the displacement solutions; and in the finite element model, this is the default frequency response output. Since this excitation is symmetric about the longitudinal axis, there is no circumferential displacement. Figure 4.2.1 shows the longitudinal displacement of the shell. As expected, there is no displacement at the $z = 0$ location of the shell. Figure 4.2.2 shows the radial displacement of the shell. The radial displacement is symmetric about the $z = 0$ location on the shell, and the maximum radial shell displacement is located near the shell and plate interface. The propagating waves reflecting off the plate and back into the shell enter the shell with the same phase angle. These propagating waves do not have the same wavenumber; therefore, they are not in phase for most of the shell. Secondary peaks can be observed where some of the waves propagating in the structure regain the same phase angle. The wave propagation model matches the finite element model well.

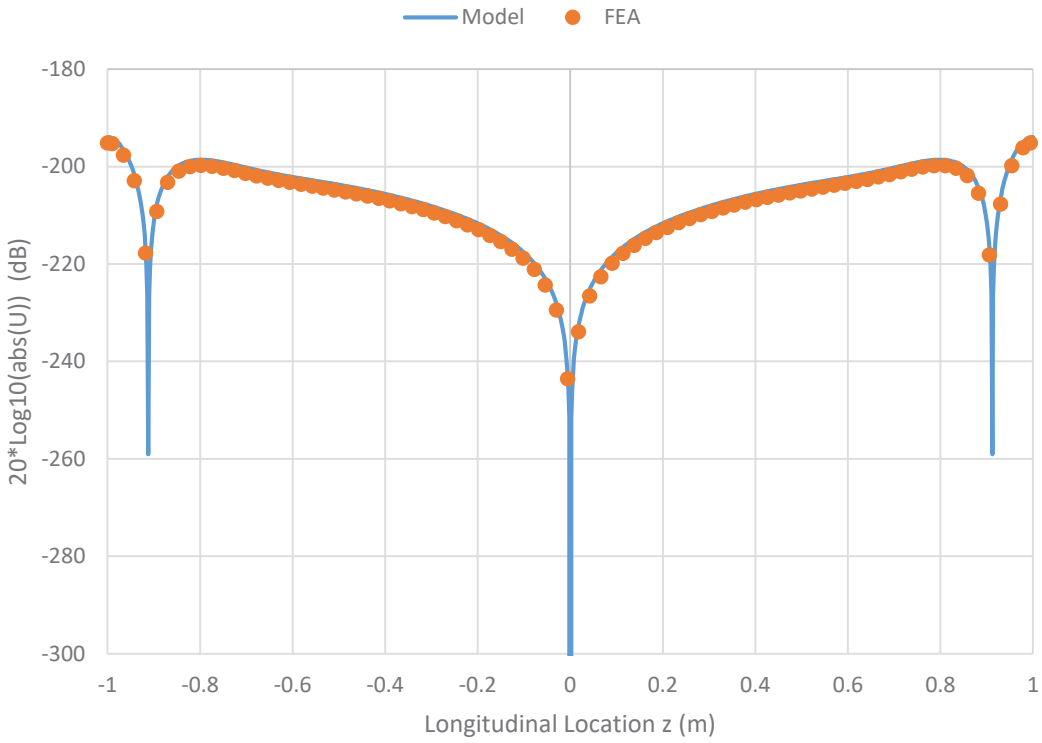

Figure 4.2.1 – Comparison between wave propagation model and finite element model for a ring excitation in the longitudinal direction

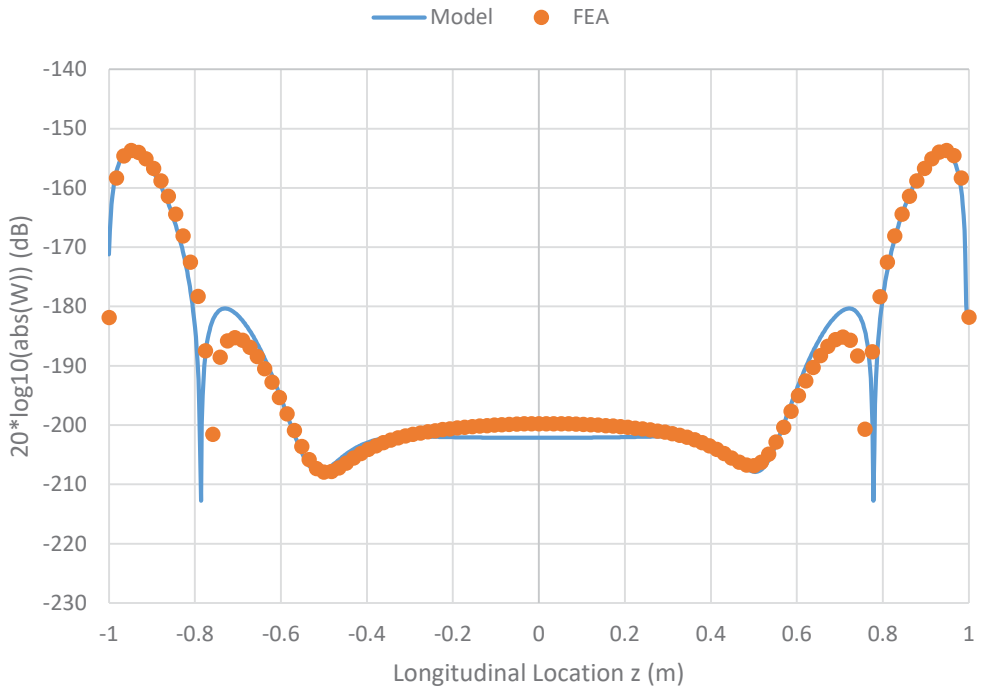

Figure 4.2.2 – Comparison between wave propagation model and finite element model for a ring excitation in the radial direction

Table 4.2.1 – Parameters specific to the wave propagation method

Parameter	Description	Value	Units
npts	Number of circumferential modes used in the wave propagation method to determine the displacement solutions (dependent on excitation).	1 or 101	-
zpts	Number of longitudinal locations used in evaluating the displacement solutions for plotting.	1001	-

4.3 Validation of the Broadside Plane Wave

A comparison of the wave propagation model and the finite element model is shown in Figures 4.3.1 and 4.3.2. This is the first of the loading conditions that can excite circumferential modes; therefore, a number of circumferential modes must be used in the wave propagation solution for the solution to converge. The displacement field solutions in Figures 4.3.1 and 4.3.2

are similar to those for the ring load as there is zero longitudinal displacement at $z = 0$ and radial displacement peaks near the shell and plate interfaces.

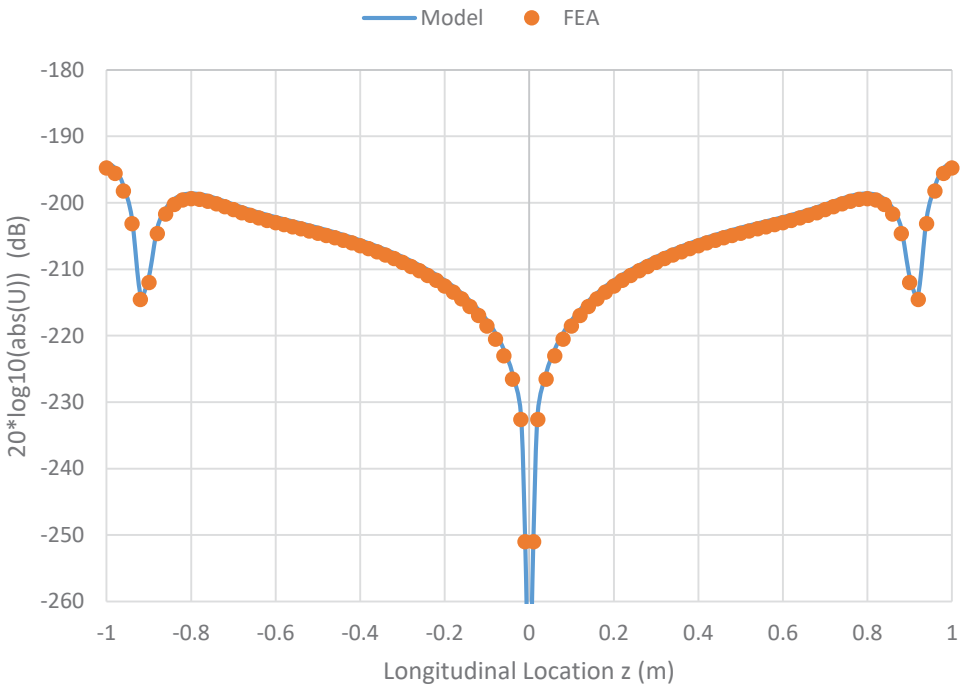

Figure 4.3.1 – Comparison between wave propagation model and finite element model for a broadside plane wave in the longitudinal direction

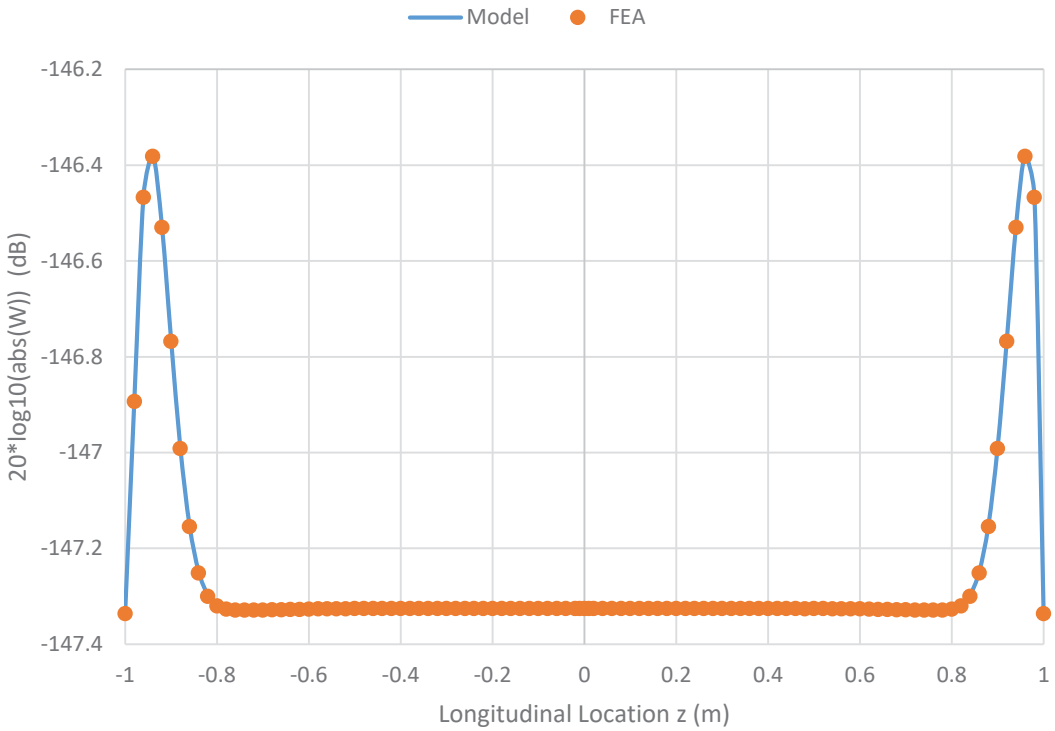

Figure 4.3.2 – Comparison between wave propagation model and finite element model for a broadside plane wave in the radial direction

4.4 Validation of the Frontside Plane Wave

A comparison of the wave propagation model and the finite element model for the longitudinal and radial directions is shown in Figures 4.4.1 and 4.4.2. Again the two models match very well. The maximum displacement in the longitudinal direction occurs at the shell and plate interfaces, and the maximum displacement in the radial direction is located just inside the plate shell interfaces. The magnitude of the longitudinal displacement in Figure 4.4.1 is near constant and more than 10 dB higher than the maximum radial displacement magnitude in Figure 4.4.2. This is expected as the frontside plate wave is a symmetric excitation propagating in the longitudinal direction.

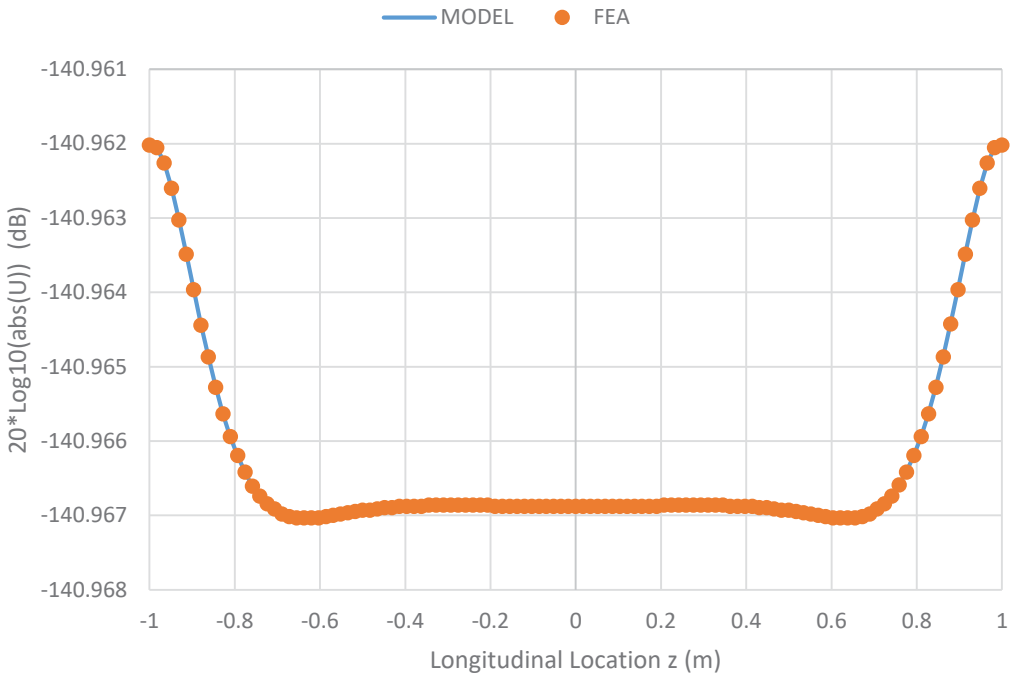

Figure 4.4.1 – Comparison between wave propagation model and finite element model for a frontside plane wave in the longitudinal direction

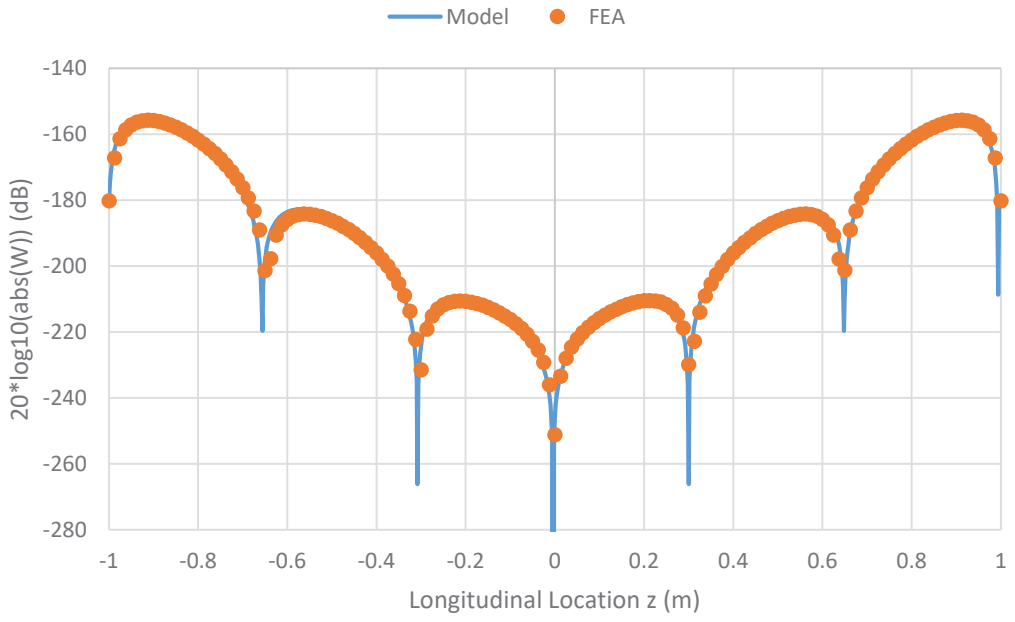

Figure 4.4.2 – Comparison between wave propagation model and finite element model for a frontside plane wave in the radial direction

4.5 Validation of the General Plane Wave

A comparison of the wave propagation model and the finite element model is shown in Figures 4.5.1 and 4.5.2. The results for the general plane wave are different than the other cases. Note the radial displacement peak only exists on the left side of Figure 4.5.2. The corresponding peak on the right side of the shell occurs at $\theta = 180^{\circ}$. The minimal longitudinal displacement in Figure 4.5.1 no longer occurs at $z = 0$. These asymmetric results should be expected as this is the only asymmetric loading condition observed in this research effort.

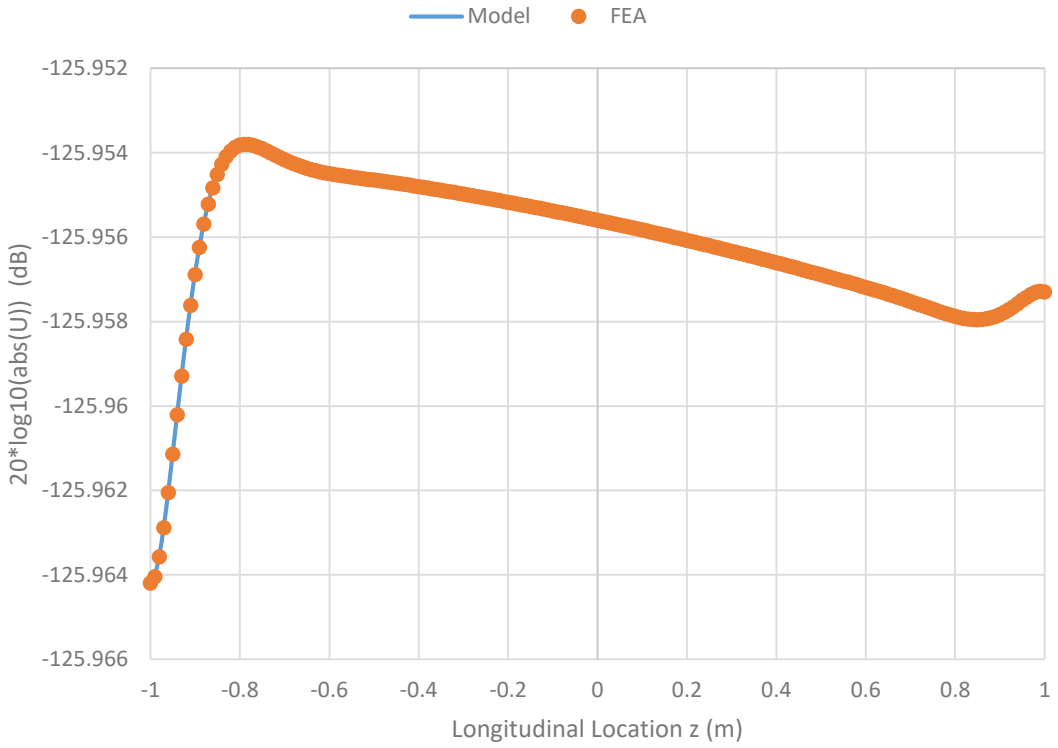

Figure 4.5.1 – Comparison between wave propagation model and finite element model for an incident plane wave in the longitudinal direction

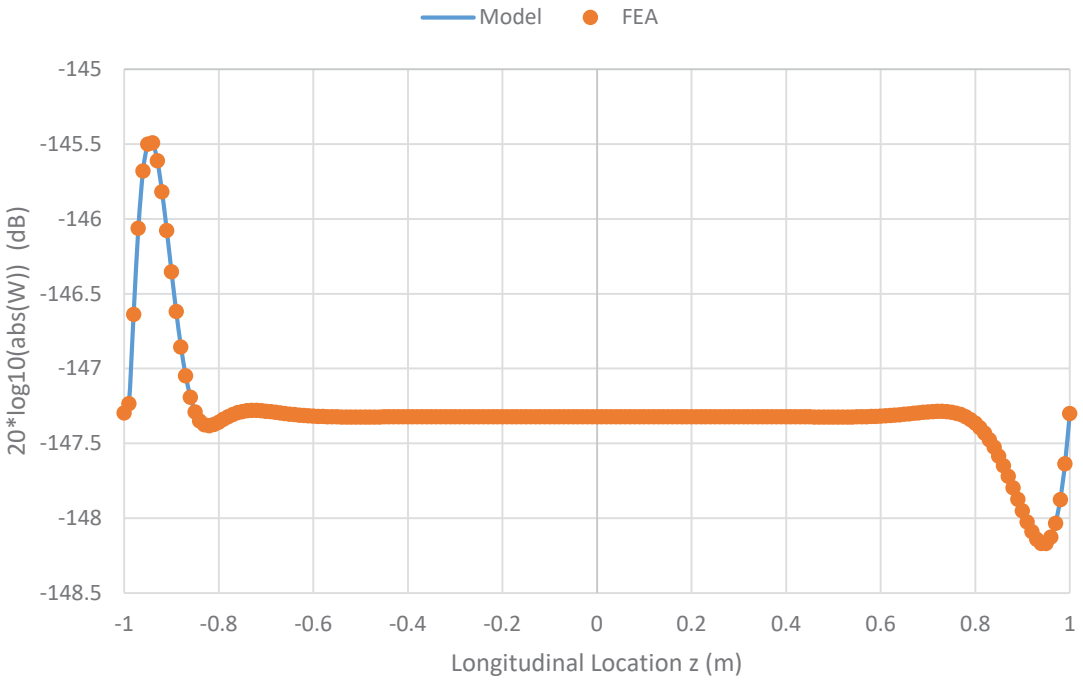

Figure 4.5.2 – Comparison between wave propagation model and finite element model for an incident plane wave in the radial direction

From the figures in this section and the previous sections, it is clear the wave propagation model has been expanded to accurately represent the distributed loading conditions outlined in section 1.1.2.

Chapter 5
Conclusions and Future Work

5.1 Conclusions

This research effort has expanded the wave propagation method of determining displacement field solutions for cylindrical shells to determine the response of a finite shell with flat plate endcaps due to complex loading conditions. The displacement results of the model have been validated via a finite element model for each type of loading condition considered, and the results of the model over a range of frequencies has been discussed. The process of characterizing loading conditions as generalized forces and moments proved to be an efficient way to apply the excitations to the system. When compared to other simpler models, the wave reflections caused by the endcaps on the shell prove to be quite complex.

5.2 Future Work

This project provides a stepping stone to apply the techniques currently used in infinitely long shell models such as acoustic coatings and reinforcing stiffeners to finite shell models while maintaining the ability to determine displacement field solutions due to complex excitations. Hemispherical endcaps and elliptical shells are also a possible addition to the capabilities of the model. The end goal of the research done after what has been discussed in this report is to create a model of a finite cylindrical shell with an acoustic coating, flat or hemispherical endcaps, and reinforcing ribs using the Navier-Cauchy fully elastic equations of motion without any simplifying

assumptions. This final model will be able to compute displacement field solutions due to a number of loading conditions.

References

1. Gould, P. *Analysis of Plates and Shells*, Springer-Verlag, New York, NY (1988).

2. Graff, K. *Wave Motion in Elastic Solids*, Dover Publications, New York, NY (1975).

3. Leissa, A. *Vibrations of Shells*, NASA, Washington, United States (1973).

4. Smith, B. Free Vibration of circular cylindrical shells of finite length, *AIAA Journal*, 8 (3), 601-603, (1970).

5. Smith, B. Vibration of a circular cylindrical shell closed by an elastic plate, *AIAA Journal*, 5 (11), 2080-2082, (1967).

6. Yuan, J. The free vibration of circularly cylindrical shell and plate systems, *Journal of Sound and Vibration*, 175 (2), 241-263, (1994).

7. Zhang, G. Free and forced vibration characteristics of submerged finite elliptic cylindrical shell, *Ocean Engineering*, 129, 92-106, (2017).

8. Caresta, M. Purely axial vibration of thin cylindrical shells with shear-diaphragm boundary conditions, *Applied Acoustics*, 70, 1081-1086 (2009).

9. Caresta, M. Acoustic signature of a submarine hull under harmonic excitation, *Applied Acoustics*, 71, 17-31, (2017).

10. Smith, P. Structural wave reflection coefficients of cylindrical shell terminations: Numerical extraction and reciprocity constraints, *J. Acoust. Soc. Am.*, 101 (2), 900-908, (1997).

11. Hull, A. An analytical model of a curved beam with a T shaped cross section, *Journal of Sound and Vibration*, 416, 29-54, (2018).

12. Ebenezer, D. Free and forced vibrations of hollow elastic cylinders of finite length, *J. Acoust. Soc. Am.*, 137 (5), 2927-2938, (2015).

13. Hull, A. Response of a cylindrical shell with finite length ring stiffeners, *Intl. Journal of Acoustics and Vibration*, 21 (3), 317-326, (2010).

14. Hull, A. Scattering from an infinite cylinder with an external fluid load – thin shell and fully elastic theory, Naval Undersea Warfare Center, Newport, RI (2016).

15. Doherty, C. Elastic response of acoustic coating on fluid-loaded rib-stiffened cylindrical shells (Master's Thesis), (2017) Retrieved from http://hdl.handle.net/10919/78288

16. Plakhov, D. Propagation of a spherical sound wave near the surface of an infinite cylindrical shell, *Soviet Physics*, 20 (6), 542-546, (1975).

17. Yu, Y. Vibrations of thin cylindrical shells analyzed by means of Donnell-type equations, *Journal of the Aero/Space Sciences*, 699-715, (1958).

18. Fang, M. Free vibration characteristics of a finite ring-stiffened elliptic cylindrical shell, *Journal of Vibration and Acoustics*, 139, (2017).

19. Donnell, L. Stability of thin-walled tubes under torsion, National Advisory Committee for Aeronautics Report Number 479, Washington, DC (1933).

20. Vinson, J. *The Behavior of Shells Composed of Isotropic and Composite Materials*, Kluwer Academic Publishers, Dordrecht, The Netherlands, (1993).

21. Cauchy, A. On the pressure or tension in a solid body, *Exercises in Mathematics*, 2, 42-56, (1827).

22. Love, A. The small free vibrations and deformation of a thin elastic shell, *Philosophical Transactions of the Royal Society of London A, Mathematical, Physical, and Engineering Sciences Royal Society*, 17, 491-549, (1888).

23. Leissa, A. *Vibrations of Plates*, NASA, Washington, United States (1969).

24. MATLAB Release 2017b, The MathWorks, Inc., Natick, MA, USA.

25. Advanpix Multiprecision Computing Toolbox, Advanpix LLC, Yokohama, Japan.

Appendix A – Matrix Entries

The nonzero entries of $\boldsymbol{A}_n$ in equation 3.1.59 are as follows:

```
A( 1, 1) = -Ds * lambda1 * ( (n^2/a^2)*(2-nu) - lambda1^2 ) * exp(lambda1*zL);
A( 1, 2) = -Ds * lambda2 * ( (n^2/a^2)*(2-nu) - lambda2^2 ) * exp(lambda2*zL);
A( 1, 3) = -Ds * lambda3 * ( (n^2/a^2)*(2-nu) - lambda3^2 ) * exp(lambda3*zL);
A( 1, 4) = -Ds * lambda4 * ( (n^2/a^2)*(2-nu) - lambda4^2 ) * exp(lambda4*zL);
A( 1, 5) = -Ds * lambda5 * ( (n^2/a^2)*(2-nu) - lambda5^2 ) * exp(lambda5*zL);
A( 1, 6) = -Ds * lambda6 * ( (n^2/a^2)*(2-nu) - lambda6^2 ) * exp(lambda6*zL);
A( 1, 7) = -Ds * lambda7 * ( (n^2/a^2)*(2-nu) - lambda7^2 ) * exp(lambda7*zL);
A( 1, 8) = -Ds * lambda8 * ( (n^2/a^2)*(2-nu) - lambda8^2 ) * exp(lambda8*zL);

A( 1, 9) = b*(E*kp/(a*(1+nu))) * besselj(n+1,kp*a) - ...
   (E*((n-n^2)*(1-nu)+kp^2*a^2)/(a^2*(1-nu^2))) * besselj(n,kp*a);
A( 1,10) = b*(-E*n*ks/(a*(1+nu))) * besselj(n+1,ks*a) + ...
   (E*n*(n-1)/(a^2*(1+nu))) * besselj(n,ks*a);

A( 2, 1) = -((-E*h*(Ku1*n - Kv1*a*lambda1))/(2*a*(1+nu))) + ...
   ( (Ds*lambda1*n*(1-nu)) / a^2 ) * exp(lambda1*zL);
A( 2, 2) = -((-E*h*(Ku2*n - Kv2*a*lambda2))/(2*a*(1+nu))) + ...
   ( (Ds*lambda2*n*(1-nu)) / a^2 ) * exp(lambda2*zL);
A( 2, 3) = -((-E*h*(Ku3*n - Kv3*a*lambda3))/(2*a*(1+nu))) + ...
   ( (Ds*lambda3*n*(1-nu)) / a^2 ) * exp(lambda3*zL);
A( 2, 4) = -((-E*h*(Ku4*n - Kv4*a*lambda4))/(2*a*(1+nu))) + ...
   ( (Ds*lambda4*n*(1-nu)) / a^2 ) * exp(lambda4*zL);
A( 2, 5) = -((-E*h*(Ku5*n - Kv5*a*lambda5))/(2*a*(1+nu))) + ...
   ( (Ds*lambda5*n*(1-nu)) / a^2 ) * exp(lambda5*zL);
A( 2, 6) = -((-E*h*(Ku6*n - Kv6*a*lambda6))/(2*a*(1+nu))) + ...
```

```
   ( (Ds*lambda6*n*(1-nu)) / a^2 ) * exp(lambda6*zL);
A( 2, 7) = -((-E*h*(Ku7*n - Kv7*a*lambda7))/(2*a*(1+nu))) + ...
   ( (Ds*lambda7*n*(1-nu)) / a^2 ) * exp(lambda7*zL);
A( 2, 8) = -((-E*h*(Ku8*n - Kv8*a*lambda8))/(2*a*(1+nu))) + ...
   ( (Ds*lambda8*n*(1-nu)) / a^2 ) * exp(lambda8*zL);

A( 2, 9) = b*(2*G*n*kp/a) * besselj(n+1,kp*a) + ...
   (-2*G*n*(n-1)/a^2) * besselj(n,kp*a);
A( 2,10) = b*(-2*G*ks/a) * besselj(n+1,ks*a) + ...
   (G*(ks^2*a^2-2*(n^2-n))/a^2) * besselj(n,ks*a);

A( 3, 1) = -(E*h*(nu + Ku1*a*lambda1 + Kv1*n*nu))/(a*(1-nu^2)) * exp(lambda1*zL);
A( 3, 2) = -(E*h*(nu + Ku2*a*lambda2 + Kv2*n*nu))/(a*(1-nu^2)) * exp(lambda2*zL);
A( 3, 3) = -(E*h*(nu + Ku3*a*lambda3 + Kv3*n*nu))/(a*(1-nu^2)) * exp(lambda3*zL);
A( 3, 4) = -(E*h*(nu + Ku4*a*lambda4 + Kv4*n*nu))/(a*(1-nu^2)) * exp(lambda4*zL);
A( 3, 5) = -(E*h*(nu + Ku5*a*lambda5 + Kv5*n*nu))/(a*(1-nu^2)) * exp(lambda5*zL);
A( 3, 6) = -(E*h*(nu + Ku6*a*lambda6 + Kv6*n*nu))/(a*(1-nu^2)) * exp(lambda6*zL);
A( 3, 7) = -(E*h*(nu + Ku7*a*lambda7 + Kv7*n*nu))/(a*(1-nu^2)) * exp(lambda7*zL);
A( 3, 8) = -(E*h*(nu + Ku8*a*lambda8 + Kv8*n*nu))/(a*(1-nu^2)) * exp(lambda8*zL);

A( 3,11) = ( (-Dp*eta/a^2) * (n^2*(1-nu) + eta^2*a^2) )  * besselj(n+1,eta*a) + ...
   ( (Dp*n/a^3) * (n*(n-1)*(1-nu) + eta^2*a^2) ) * besselj(n,eta*a);
A( 3,12) = ( ( Dp*eta/a^2) * (n^2*(1-nu) - eta^2*a^2) )  * besseli(n+1,eta*a) + ...
   ( (Dp*n/a^3) * (n*(n-1)*(1-nu) - eta^2*a^2) ) * besseli(n,eta*a);

A( 4, 1) = -Ds * (((n^2*nu)/a^2) - lambda1^2) * exp(lambda1*zL);
A( 4, 2) = -Ds * (((n^2*nu)/a^2) - lambda2^2) * exp(lambda2*zL);
A( 4, 3) = -Ds * (((n^2*nu)/a^2) - lambda3^2) * exp(lambda3*zL);
```

```
A( 4, 4) = -Ds * (((n^2*nu)/a^2) - lambda4^2) * exp(lambda4*zL);
A( 4, 5) = -Ds * (((n^2*nu)/a^2) - lambda5^2) * exp(lambda5*zL);
A( 4, 6) = -Ds * (((n^2*nu)/a^2) - lambda6^2) * exp(lambda6*zL);
A( 4, 7) = -Ds * (((n^2*nu)/a^2) - lambda7^2) * exp(lambda7*zL);
A( 4, 8) = -Ds * (((n^2*nu)/a^2) - lambda8^2) * exp(lambda8*zL);

A( 4,11) = (-Dp*eta*(1-nu)/a)                    * besselj(n+1,eta*a) + ...
   (-Dp/a^2) * (n*(n-1)*(1-nu) - eta^2*a^2) * besselj(n,eta*a);
A( 4,12) = ( Dp*eta*(1-nu)/a)                    * besseli(n+1,eta*a) + ...
   (-Dp/a^2) * (n*(n-1)*(1-nu) + eta^2*a^2) * besseli(n,eta*a);

A( 5, 1) = -Ku1 * exp(lambda1*zL);
A( 5, 2) = -Ku2 * exp(lambda2*zL);
A( 5, 3) = -Ku3 * exp(lambda3*zL);
A( 5, 4) = -Ku4 * exp(lambda4*zL);
A( 5, 5) = -Ku5 * exp(lambda5*zL);
A( 5, 6) = -Ku6 * exp(lambda6*zL);
A( 5, 7) = -Ku7 * exp(lambda7*zL);
A( 5, 8) = -Ku8 * exp(lambda8*zL);

A( 5,11) = besselj(n,eta*a);
A( 5,12) = besseli(n,eta*a);

A( 6, 1) = -Kv1 * exp(lambda1*zL);
A( 6, 2) = -Kv2 * exp(lambda2*zL);
A( 6, 3) = -Kv3 * exp(lambda3*zL);
A( 6, 4) = -Kv4 * exp(lambda4*zL);
A( 6, 5) = -Kv5 * exp(lambda5*zL);
```

```
A( 6, 6) = -Kv6 * exp(lambda6*zL);
A( 6, 7) = -Kv7 * exp(lambda7*zL);
A( 6, 8) = -Kv8 * exp(lambda8*zL);

A( 6, 9) = (-n/a) * besselj(n,kp*a);
A( 6,10) = ks*besselj(n+1,ks*a) - (n/a)*besselj(n,ks*a);

A( 7, 1) = -1 * exp(lambda1*zL);
A( 7, 2) = -1 * exp(lambda2*zL);
A( 7, 3) = -1 * exp(lambda3*zL);
A( 7, 4) = -1 * exp(lambda4*zL);
A( 7, 5) = -1 * exp(lambda5*zL);
A( 7, 6) = -1 * exp(lambda6*zL);
A( 7, 7) = -1 * exp(lambda7*zL);
A( 7, 8) = -1 * exp(lambda8*zL);

A( 7, 9) = (-kp)*besselj(n+1,kp*a) + (n/a)*besselj(n,kp*a);
A( 7,10) = (n/a) * besselj(n,ks*a);

A( 8, 1) = lambda1 * exp(lambda1*zL);
A( 8, 2) = lambda2 * exp(lambda2*zL);
A( 8, 3) = lambda3 * exp(lambda3*zL);
A( 8, 4) = lambda4 * exp(lambda4*zL);
A( 8, 5) = lambda5 * exp(lambda5*zL);
A( 8, 6) = lambda6 * exp(lambda6*zL);
A( 8, 7) = lambda7 * exp(lambda7*zL);
A( 8, 8) = lambda8 * exp(lambda8*zL);
```

```
A( 8,11) = -eta*besselj(n+1,eta*a) + (n/a)*besselj(n,eta*a);
A( 8,12) =  eta*besseli(n+1,eta*a) + (n/a)*besseli(n,eta*a);

A( 9, 1) = Ds * lambda1 * ( (n^2/a^2)*(2-nu) - lambda1^2 ) * exp(lambda1*zR);
A( 9, 2) = Ds * lambda2 * ( (n^2/a^2)*(2-nu) - lambda2^2 ) * exp(lambda2*zR);
A( 9, 3) = Ds * lambda3 * ( (n^2/a^2)*(2-nu) - lambda3^2 ) * exp(lambda3*zR);
A( 9, 4) = Ds * lambda4 * ( (n^2/a^2)*(2-nu) - lambda4^2 ) * exp(lambda4*zR);
A( 9, 5) = Ds * lambda5 * ( (n^2/a^2)*(2-nu) - lambda5^2 ) * exp(lambda5*zR);
A( 9, 6) = Ds * lambda6 * ( (n^2/a^2)*(2-nu) - lambda6^2 ) * exp(lambda6*zR);
A( 9, 7) = Ds * lambda7 * ( (n^2/a^2)*(2-nu) - lambda7^2 ) * exp(lambda7*zR);
A( 9, 8) = Ds * lambda8 * ( (n^2/a^2)*(2-nu) - lambda8^2 ) * exp(lambda8*zR);

A( 9,13) = b*(E*kp/(a*(1+nu))) * besselj(n+1,kp*a) - ...
   (E*((n-n^2)*(1-nu)+kp^2*a^2)/(a^2*(1-nu^2))) * besselj(n,kp*a);
A( 9,14) = b*(-E*n*ks/(a*(1+nu))) * besselj(n+1,ks*a) + ...
   (E*n*(n-1)/(a^2*(1+nu))) * besselj(n,ks*a);

A(10, 1) = ((-E*h*(Ku1*n - Kv1*a*lambda1))/(2*a*(1+nu))) + ...
   ( (Ds*lambda1*n*(1-nu)) / a^2 ) * exp(lambda1*zR);
A(10, 2) = ((-E*h*(Ku2*n - Kv2*a*lambda2))/(2*a*(1+nu))) + ...
   ( (Ds*lambda2*n*(1-nu)) / a^2 ) * exp(lambda2*zR);
A(10, 3) = ((-E*h*(Ku3*n - Kv3*a*lambda3))/(2*a*(1+nu))) + ...
   ( (Ds*lambda3*n*(1-nu)) / a^2 ) * exp(lambda3*zR);
A(10, 4) = ((-E*h*(Ku4*n - Kv4*a*lambda4))/(2*a*(1+nu))) + ...
   ( (Ds*lambda4*n*(1-nu)) / a^2 ) * exp(lambda4*zR);
A(10, 5) = ((-E*h*(Ku5*n - Kv5*a*lambda5))/(2*a*(1+nu))) + ...
   ( (Ds*lambda5*n*(1-nu)) / a^2 ) * exp(lambda5*zR);
A(10, 6) = ((-E*h*(Ku6*n - Kv6*a*lambda6))/(2*a*(1+nu))) + ...
```

```
   ( (Ds*lambda6*n*(1-nu)) / a^2 ) * exp(lambda6*zR);
A(10, 7) = ((-E*h*(Ku7*n - Kv7*a*lambda7))/(2*a*(1+nu))) + ...
   ( (Ds*lambda7*n*(1-nu)) / a^2 ) * exp(lambda7*zR);
A(10, 8) = ((-E*h*(Ku8*n - Kv8*a*lambda8))/(2*a*(1+nu))) + ...
   ( (Ds*lambda8*n*(1-nu)) / a^2 ) * exp(lambda8*zR);

A(10,13) = b*(2*G*n*kp/a) * besselj(n+1,kp*a) + ...
   (-2*G*n*(n-1)/a^2) * besselj(n,kp*a);
A(10,14) = b*(-2*G*ks/a) * besselj(n+1,ks*a) + ...
   (G*(ks^2*a^2-2*(n^2-n))/a^2) * besselj(n,ks*a);

A(11, 1) = (E*h*(nu + Ku1*a*lambda1 + Kv1*n*nu))/(a*(1-nu^2)) * exp(lambda1*zR);
A(11, 2) = (E*h*(nu + Ku2*a*lambda2 + Kv2*n*nu))/(a*(1-nu^2)) * exp(lambda2*zR);
A(11, 3) = (E*h*(nu + Ku3*a*lambda3 + Kv3*n*nu))/(a*(1-nu^2)) * exp(lambda3*zR);
A(11, 4) = (E*h*(nu + Ku4*a*lambda4 + Kv4*n*nu))/(a*(1-nu^2)) * exp(lambda4*zR);
A(11, 5) = (E*h*(nu + Ku5*a*lambda5 + Kv5*n*nu))/(a*(1-nu^2)) * exp(lambda5*zR);
A(11, 6) = (E*h*(nu + Ku6*a*lambda6 + Kv6*n*nu))/(a*(1-nu^2)) * exp(lambda6*zR);
A(11, 7) = (E*h*(nu + Ku7*a*lambda7 + Kv7*n*nu))/(a*(1-nu^2)) * exp(lambda7*zR);
A(11, 8) = (E*h*(nu + Ku8*a*lambda8 + Kv8*n*nu))/(a*(1-nu^2)) * exp(lambda8*zR);

A(11,15) = ( (-Dp*eta/a^2) * (n^2*(1-nu) + eta^2*a^2) )  * besselj(n+1,eta*a) + ...
   ( (Dp*n/a^3) * (n*(n-1)*(1-nu) + eta^2*a^2) ) * besselj(n,eta*a);
A(11,16) = ( ( Dp*eta/a^2) * (n^2*(1-nu) - eta^2*a^2) )  * besseli(n+1,eta*a) + ...
   ( (Dp*n/a^3) * (n*(n-1)*(1-nu) - eta^2*a^2) ) * besseli(n,eta*a);

A(12, 1) = Ds * (((n^2*nu)/a^2) - lambda1^2) * exp(lambda1*zR);
A(12, 2) = Ds * (((n^2*nu)/a^2) - lambda2^2) * exp(lambda2*zR);
A(12, 3) = Ds * (((n^2*nu)/a^2) - lambda3^2) * exp(lambda3*zR);
```

```
A(12, 4) = Ds * (((n^2*nu)/a^2) - lambda4^2) * exp(lambda4*zR);
A(12, 5) = Ds * (((n^2*nu)/a^2) - lambda5^2) * exp(lambda5*zR);
A(12, 6) = Ds * (((n^2*nu)/a^2) - lambda6^2) * exp(lambda6*zR);
A(12, 7) = Ds * (((n^2*nu)/a^2) - lambda7^2) * exp(lambda7*zR);
A(12, 8) = Ds * (((n^2*nu)/a^2) - lambda8^2) * exp(lambda8*zR);

A(12,15) = (-Dp*eta*(1-nu)/a)                    * besselj(n+1,eta*a) + ...
   (-Dp/a^2) * (n*(n-1)*(1-nu) - eta^2*a^2) * besselj(n,eta*a);
A(12,16) = ( Dp*eta*(1-nu)/a)                    * besseli(n+1,eta*a) + ...
   (-Dp/a^2) * (n*(n-1)*(1-nu) + eta^2*a^2) * besseli(n,eta*a);

A(13, 1) = -Ku1 * exp(lambda1*zR);
A(13, 2) = -Ku2 * exp(lambda2*zR);
A(13, 3) = -Ku3 * exp(lambda3*zR);
A(13, 4) = -Ku4 * exp(lambda4*zR);
A(13, 5) = -Ku5 * exp(lambda5*zR);
A(13, 6) = -Ku6 * exp(lambda6*zR);
A(13, 7) = -Ku7 * exp(lambda7*zR);
A(13, 8) = -Ku8 * exp(lambda8*zR);

A(13,15) = besselj(n,eta*a);
A(13,16) = besseli(n,eta*a);

A(14, 1) = -Kv1 * exp(lambda1*zR);
A(14, 2) = -Kv2 * exp(lambda2*zR);
A(14, 3) = -Kv3 * exp(lambda3*zR);
A(14, 4) = -Kv4 * exp(lambda4*zR);
A(14, 5) = -Kv5 * exp(lambda5*zR);
```

```
A(14, 6) = -Kv6 * exp(lambda6*zR);
A(14, 7) = -Kv7 * exp(lambda7*zR);
A(14, 8) = -Kv8 * exp(lambda8*zR);

A(14,13) = (-n/a) * besselj(n,kp*a);
A(14,14) = ks*besselj(n+1,ks*a) - (n/a)*besselj(n,ks*a);

A(15, 1) = -1 * exp(lambda1*zR);
A(15, 2) = -1 * exp(lambda2*zR);
A(15, 3) = -1 * exp(lambda3*zR);
A(15, 4) = -1 * exp(lambda4*zR);
A(15, 5) = -1 * exp(lambda5*zR);
A(15, 6) = -1 * exp(lambda6*zR);
A(15, 7) = -1 * exp(lambda7*zR);
A(15, 8) = -1 * exp(lambda8*zR);

A(15,13) = (-kp)*besselj(n+1,kp*a) + (n/a)*besselj(n,kp*a);
A(15,14) = (n/a) * besselj(n,ks*a);

A(16, 1) = lambda1 * exp(lambda1*zR);
A(16, 2) = lambda2 * exp(lambda2*zR);
A(16, 3) = lambda3 * exp(lambda3*zR);
A(16, 4) = lambda4 * exp(lambda4*zR);
A(16, 5) = lambda5 * exp(lambda5*zR);
A(16, 6) = lambda6 * exp(lambda6*zR);
A(16, 7) = lambda7 * exp(lambda7*zR);
A(16, 8) = lambda8 * exp(lambda8*zR);
```

```
A(16, 15) = -eta*besselj(n+1,eta*a) + (n/a)*besselj(n,eta*a);
A(16, 16) =  eta*besseli(n+1,eta*a) + (n/a)*besseli(n,eta*a);
```